https://doi.org/10.5194/egusphere-2026-3070
Preprint. Discussion started: 3 July 2026

Entwined long-range transports of biomass burning aerosols over the South-West Indian Ocean: a case study of aerosol river in September 2017

Dominique Gantois[1], Alexandre Baron[2], Michaël Sicard[1,3], Valentin Duflot[4], Niels Groenen[1], Nelson Bègue[1], Sabine Eckhardt[4], Nikolaos Evangeliou[4], Martine De Mazière[5], Corinne Vigouroux[5], Guillaume Payen[6], Nicolas Marquestaut[6], Jean-Marc Metzger[6], Patrick Chazette[7], Cyrille Flamant[8]

[1]Laboratoire de l'Atmosphère et des Cyclones, UMR 8105 Université de La Réunion - CNRS - Météo-France, Saint Denis de La Réunion, France
[2]Cooperative Institute for Research in Environmental Sciences (CIRES), University of Colorado, Boulder, CO, USA
[3]CommSensLab-UPC, Universitat Politècnica de Catalunya, Barcelona, 08034, Spain
[4]Stiftelsen, NILU (former Norwegian Institute for Air Research), Kjeller, Norway
[5]Royal Belgian Institute for Space Aeronomy (BIRA-IASB), Ringlaan 3, B-1180, Brussels, Belgium
[6]Observatoire des Sciences de l'Univers de La Réunion (OSU-Réunion), UAR3365, Université de La Réunion, CNRS, IRD, Météo-France, 97490 Saint-Denis de La Réunion, France
[7]Laboratoire des Sciences du Climat et de l'Environnement (LSCE)/IPSL, UMR CNRS 1572, CEA, UVSQ, Gif-sur-Yvette, France
[8]Laboratoire Atmosphère Milieux Observations Spatiales (LATMOS)/IPSL, UMR CNRS 8190, Sorbonne Université, UVSQ, Paris, France

Correspondence to: Dominique Gantois (dominique.gantois@univ-reunion.fr)

Abstract. Biomass burning (BB) aerosols emitted over Southern Africa (SAF) and South America (SA) represent a major seasonal perturbation to the usually pristine atmosphere of the South-West Indian Ocean (SWIO) but remain understudied in this remote region. Following a multi-instrumental approach, we characterize BB plumes reaching Reunion Island (21°S, 55°E) during September 2017, combining ground-based measurements (sun-photometer, lidars, Fourier Transform Infrared spectrometer), spaceborne observations, CAMS EAC4 reanalysis, and the Lagrangian transport model FLEXPART. Aerosol optical depth at 550 nm over Reunion reached unusually high values (0.16-0.42) during the second half of September, with organic matter contributing up to 60 %. MODIS imagery revealed two large-scale smoke plumes originating from SAF and SA transported toward the SWIO, and CALIOP profiles showed smoke layers extending from 4 to 9 km of altitude above Madagascar. On September 19th, a single layer was identified over Reunion between 2.8 and 4.7 km with an Ångström exponent ($Å_{355/532}$) of 1.32 ± 0.23, consistent with moderately aged BB particles essentially originating from SAF. On September 25th, two vertically decoupled layers were identified: a lower layer (3.3-5 km, Å= 1.45 ± 0.12) associated with mixed aged aerosols of SAF and SA origin, and an upper, drier layer (5-9 km, Å= 1.60 ± 0.06) of potentially fresher SAF smoke, consistent with rapid convective uplift into the mid-troposphere. This study offers new insights concerning the

https://doi.org/10.5194/egusphere-2026-3070
Preprint. Discussion started: 3 July 2026

dynamical processes that govern aerosol variability over Reunion Island and highlights its value as a strategic long-term observational site in the SWIO.

1 Introduction

The Southern Hemisphere (SH) tropospheric aerosol content is characterized by a strong disparity between widespread near-pristine marine regions and seasonally polluted continental outflows. Over the oceans, background conditions are essentially made of marine aerosols such as sea salt and organic aerosols, responsible for low aerosol optical depth (AOD) values as measured over the South-West Indian Ocean (SWIO) (Mascaut et al., 2022). Over land, certain continental regions, such as Southern Africa and South America are the main seasonal sources of biomass burning (BB) aerosols (Van Der Werf et al., 2017). During the BB season (May - October, (Edwards et al., 2006)), the dry season in the tropics, massive fires emit large quantities of carbonaceous particles such as black carbon (BC) and organic matter (OM). These emissions create elevated smoke layers in the free troposphere (at typically 3, 5 and 8 km for African fires, (Edwards et al., 2006; Garstang et al., 1996; Ranaivombola et al., 2023)). These layers can follow long-range transport routes across the Atlantic and Indian Oceans (Edwards et al., 2006; Garstang et al., 1996; Thompson et al., 1996), leading to seasonal peaks in AOD (Ranaivombola et al., 2023), and inducing radiative effects related to absorption and aerosol-cloud interaction (Lu et al., 2018). Therefore, the SH troposphere could be represented as a two-regime system, with an aerosol background content made of clean marine aerosols, seasonally affected by short- and long-range transported BB aerosols.

Our understanding of this system has and is still being improved thanks to several major multi-instrumental international field campaigns that provided observations leading to key findings in terms of aerosol emissions, transport, and radiative effect. The SAFARI (Southern African Regional Science Initiative) 2000 campaign (Swap et al., 2003) was one of the first large-scale observational campaign designed to study BB aerosols over Southern Africa. It showed that BB is the main source of aerosols and trace gases in this region, and datasets from this campaign became benchmarks for global fire emission inventories (GFED, Global Fire Emission Database). It also revealed the existence of extensive regional smoke layers above Southern Africa and introduced the concept of "river of smoke" corresponding to a large-scale smoke plume transported from Southern Africa toward the Indian Ocean, highlighting the efficiency of continental to ocean aerosol export (Schmid et al., 2003). The INDOEX campaign (Ramanathan et al., 2001) focused on anthropogenic pollution from South-East Asia spreading over the Indian Ocean and showed that continental outflow from South-East Asia strongly perturbs the radiative balance of otherwise pristine marine environments, sometimes thousands of kilometers away. These effects can influence large-scale systems such as the South Asian Monsoon. More recently, the AEROCLO-sA campaign (Formenti et al., 2019) focused on BB aerosols over Southern Africa and the southeast Atlantic. It followed a multi-instrumental coordinated approach by using aircraft, ground-based, and satellite observations to investigate aerosol vertical distribution, aerosol-cloud overlap, and radiative effects. This campaign confirmed the persistence of elevated smoke layers, highlighting the role of dynamical transport in shaping aerosol stratification, and demonstrated how absorbing aerosols can modify atmospheric stability and cloud development. It

https://doi.org/10.5194/egusphere-2026-3070
Preprint. Discussion started: 3 July 2026

led to understand that aerosol transport along the Namibian coast is highly variable and vertically structured, with multiple layers of smoke from Angola and dust from South America extending through the lower and mid-troposphere under the influence of changing synoptic circulations such as coastal flows, jets, and cut-off lows (Chazette et al., 2019). With the help of global and mesoscale numerical simulations, another study (Flamant et al., 2022) focused on a coherent, fast-moving "river of smoke", travelling for thousands of kilometers from Southern Africa toward the southeast Atlantic and Indian Ocean, and transporting BB aerosols. It showed that this long-range transport is driven by coupled synoptic-scale systems (tropical easterly disturbances, midlatitude westerly waves, and cut-off lows forming tropical-temperate troughs) which efficiently lift smoke into the mid- and upper troposphere (sometimes up to 8 km) and channel it along well-defined atmospheric pathways. More recently, (Ranaivombola et al., 2025) documented "river of smoke" events over the SWIO during the BB Aerosol Campaign (BiBAC) at Skukuza (South Africa), but under different synoptic conditions from those previously described. This work highlighted the diversity of large-scale dynamical pathways capable of channeling BB aerosols from Southern Africa toward the SWIO. These organized transport corridors are key for exporting aerosols far from their sources and strongly influence their radiative and cloud impacts downstream.

All of these campaigns demonstrate that the observed aerosol climatology in the SH strongly depend on organized, multi-scale processes involving emission, uplift, and long-range transport. Despite the progress already achieved, significant uncertainties remain in the quantification of aerosol radiative forcing in remote marine environments such as the SWIO, both through direct radiative effects and indirect effects on cloud microphysics. Reducting these uncertainties is a challenge compounded by the relative scarcity of long-term, high-resolution observational datasets in this region. This challenge is also amplified by the intensification of wildfire activity in the SH. In fact, recent analyses show that fire numbers and cumulated intensities across South America have been rising significantly over the past two decades (Groenen et al., 2026).

In this context, Reunion Island (21°S, 55°E) emerges as a unique strategic observational site in the SH. Located in the SWIO, it hosts the Observatory of Atmospheric Physics of La Reunion (OPAR), and lies at the crossing of major atmospheric transport pathways linking Southern Africa, South America, Southern and Southeast Asia (Duflot et al., 2022). This location enables the island to observe both **(i)** clean marine background conditions dominated by marine aerosols under the influence of trade-winds (Mascaut et al., 2022), and **(ii)** seasonal perturbations associated with long-range transported biomass burning plumes (Duflot et al., 2022). The high-altitude Maïdo Observatory (2160 m asl, (Baray et al., 2013)) provides direct access to the free troposphere. It hosts several ground-based instruments that can help study tropospheric aerosol content, validate satellite retrievals, and evaluate transport models. These instruments include sun-photometers to measure total aerosol optical depth (AOD), multiwavelength UV and visible lidars to retrieve vertical profiles of aerosol optical properties, and Fourier Transform Infra-red (FTIR) spectrometers to measure partial columns of Carbon Monoxide (CO) related to BB emissions.

In this work, we aim to identify the vertical structure, optical properties, and origins of BB aerosol layers reaching Reunion Island, and to assess whether a multi-instrumental approach can help reduce uncertainties in aerosol radiative forcing assessments in this understudied region of the SH. To that end, we combine ground-based measurements at Maïdo Observatory with satellite observations and transport modelling to provide a multi-instrumental approach, focusing on specific episodes of

https://doi.org/10.5194/egusphere-2026-3070
Preprint. Discussion started: 3 July 2026

seasonal BB plumes transport above Reunion Island in September 2017. We characterize the structure and optical properties of these plumes for the first time with a high vertical resolution. A Lagrangian model is then used to identify the aerosols origins and follow their transport.

2 Data and method

2.1 Instruments

2.1.1 CIMEL Sun-photometer

The total AOD_{500} and the Ångström exponent between 440 and 675 nm ($Ä_{440-675}$) were retrieved from a CIMEL sun-photometer (Cimel Electronique, Paris - France) located on a rooftop at the University of La Réunion in the city of Saint-Denis (80 m asl, 20.90°S, 55.45°E). This instrument is in the SNO PHOTON/AERONET network (Service National d'Observation PHOTONS/AErosol RObotic NETwork) (Holben et al., 1998), part of ACTRIS-ERIC (Aerosol, Clouds, Trace Gases European Research Infrastructure Consortium). The data retrieved corresponded to direct sun version 3 level 2.0 (Giles et al., 2019; Smirnov et al., 2000) and was downloaded from AERONET website (https://aeronet.gsfc.nasa.gov/cgi-bin/webtool_aod_v3, last access: April 28th, 2025). AOD level 2.0 product from the CIMEL Sun-photometer was accessed for measurements from December 2003 until December 2024. The AOD_{500} wavelength was converted into AOD_{550} wavelength and into AOD_{532} wavelength using $Ä_{440-675}$ in order to facilitate comparisons with similar variables from model reanalysis or lidar measurements at 532 nm.

2.1.2 Spaceborne instruments

2.1.2.1 MODIS

The Moderate Resolution Imaging Spectroradiometers (MODIS) are spaceborne instruments onboard the synchronous polar-orbiting platforms Terra and Aqua (King et al., 1992; Salomonson et al., 1989). Both platforms provide a quasi-complete coverage of the Earth with a vertical resolution between 250 and 1000m at ground level depending on the spectral band. In this study, we use the Terra and Aqua AOT at 550 nm from the MODIS aerosol product level 2 data (http://aqua.nasa.gov, last access: 03 Avril 2026) with a spatial resolution at nadir of 10 * 10 km^2. We also use the radiance-based Fire Radiative Power (FRP), derived from MODIS measurements on the Aqua platform. The uncertainty on the AOT is ±0.15 ±0.05 AOT over the land and ±0.05 ±0.03 AOT over the ocean (Chu et al., 2002).

2.1.2.2 CALIOP

In this study, we also use vertical profiles of aerosol optical products from the Cloud-Aerosol LIdar with Orthogonal Polarization (CALIOP) aboard Cloud-Aerosol Lidar and Infrared Pathfinder Satellite Observations (CALIPSO, http://www-calipso.larc.nasa.gov, last access: 10 April 2026). Details on this instrument and the methodology for data processing can be

https://doi.org/10.5194/egusphere-2026-3070
Preprint. Discussion started: 3 July 2026

found in (Winker et al., 2007). In this work, we use CALIOP level-2 data version 4.10 (Tackett et al., 2023). The inversion method is described in (Young and Vaughan, 2009); and the aerosol classification method can be found in (Kim et al., 2018) with updates in (Tackett et al., 2023).

2.1.3 Ground-based lidars

Two Maido lidars are used to retrieve vertical profiles of aerosol optical properties in the troposphere. The Li1200 provides Rayleigh-Mie scattering profiles at 355 nm, Raman N_2 scattering profiles at 387 nm, and Raman H_2O scattering profiles at 407 nm. The LiO3T provides elastic scattering profiles at 532 nm with polarization information, elastic scattering profiles at 1064 nm, and Raman N_2 scattering profiles at 607 nm. Technical specifications for both instruments can be found in a dedicated data paper (Gantois et al., 2024). Data can be accessed at https://doi.org/10.26171/rwcm-q370 (last access April 28th, 2025). These lidars are routinely operated twice per week and only measured during nighttime to ensure a good signal to noise ratio (SNR).

The datasets consist of 1-minute integrated profiles for the Li1200 and 2-minutes integrated profiles for the LiO3T. An overlap factor correction was applied for the very low 355 nm elastic channel of the Li1200, as well as the polarized 532 nm elastic channels of the LiO3T. Up to now, it has never been physically possible to perform horizontal measurements with Maïdo lidars. Therefore, an experimental approach using vertical measurements (instead of horizontal) in aerosol-free conditions was performed. Specifics about the equation used as well as the corresponding uncertainty analysis can be found in(Gantois et al., 2024). Concerning the retrieval of aerosol optical products, a two-component Klett inversion was applied to the time-series, initially using a constant LR value of 50 sr (Klett, 1985). The corresponding equations and uncertainties can be found in (Gantois et al., 2024). A Raman inversion was then performed for the Li1200 using the average signal for each time-series to improve the SNR for the 387 nm channel. The corresponding equations used to compute the aerosol extinction and backscatter coefficients as well as the lidar ratio (LR) profile can be found in (Ansmann et al., 1992). The mean value of this lidar ratio profile was used to perform a new Klett inversion on the lidar signal time-series. An Ångström exponent (Ä) was also derived from the aerosol backscatter at 355 nm and 532 nm.

Vertical profiles of Water vapor mixing ratio (WVMR) were retrieved from the 387 nm and 407 nm channels of the Li1200 using the methodology described in (Vérèmes et al., 2019). Time-series of WVMR vertical profiles were computed, using integrated 5-minute signals from the Li1200 as described in Eq. (5) (Whiteman et al., 2006):

$$WVMR(z) = C * O(z) * \Gamma(z) * \frac{P_{H_2O}(z) - SB_{H_2O}(z)}{P_{N_2}(z) - SB_{N_2}(z)} \Delta\tau, \quad (1)$$

where C is the calibration coefficient, $O(z)$ is the overlap function, $\Gamma(z)$ is the temperature-dependent Raman cross-sections, P_{H_2O} and P_{N_2} are respectively the power received at the 407 nm and 387 nm wavelengths, SB_{H_2O} and SB_{N_2} are respectively the sky background at the 407 nm and 387 nm wavelengths, and $\Delta\tau$ is the differential term due to the atmosphere. The calibration constant was retrieved using the GNSS (Global Navigation Satellite System) methodology described in (Vérèmes et al., 2019).

https://doi.org/10.5194/egusphere-2026-3070
Preprint. Discussion started: 3 July 2026

2.1.4 FTIR

A Bruker IFS 125HR Fourier Transform Infra-red (FTIR) spectrometer has been continuously measuring at Maïdo observatory since March 2013 (Baray et al., 2013). This instrument is equipped with two detectors: InSb and MCT, and with a KBr beamsplitter. It covers the spectral range from 600 to 4500 cm−1 (2.2 to 16 µm). with a maximum optical path difference of 257 cm. To obtain one spectrum, the instrument must provide one forward and one backward scan in less than 3 minutes. Usually, two or three scans must be averaged to increase the SNR. Vertical profiles of volume mixing ratios of CO were derived using the Optimal Estimation Method, implemented in SFIT4 (SFIT4:V0.9.4.4, https://wiki.ucar.edu/display/sfit4/Infrared+Working+Group+Retrieval+Code%2C+SFIT, (Hannigan et al., 2024)). Details on the CO retrieval settings can be found in (Zhou et al., 2018), including the fitted spectral windows, interfering species, and averaging kernels description. Concerning ancillary data, a priori temperature and pressure profiles were derived from 6-hourly NCEP analyses from the surface up to 1 mbar altitude, and WACCM monthly means above. A priori profiles of CO volume mixing ratio were taken from the WACCM v6 model. Vertical profiles of volume mixing ratios of CO were weighted by the airmasses in each retrieval layer and integrated to give the total or profiles of partial columns in molecules.cm^{-2}. The uncertainty budget was based on the methodology of Rogers (Rodgers, 2000). The total uncertainty has been determined by adding all components in quadrature. In our study, we chose to extract the uncertainty profiles from the diagonal of the covariance matrices. The risk is to underestimate the uncertainty by not taking into account the potential correlation with the non-diagonal elements. The most important contributions to the random and systematic uncertainty budget are the measurement noise and the spectroscopic parameters, respectively (Senten et al., 2008). Mean random and systematic uncertainties on CO total columns are 1.2% and 2.5%, respectively. In addition to total columns, FTIR can provide low-vertical resolution CO profiles. The mean degrees-of-freedom for signal (DOFS, trace of the averaging kernel matrix) is 2.25, meaning that at least 2 independent pieces of information can be retrieved from the FTIR spectra. In the altitude used in the present study, the mean DOFS is 0.62 for the ground to 5 km range, and 1.15 for the 5 to 15 km range. The FTIR data sets can be accessed at the NDACC repository (https://ndacc.larc.nasa.gov/index.php/instruments/ftir-spectrometer/profile-multiple-species-ftir-spectrometer-bruker-125hr-reunion, last access April 29th, 2025).

A climatology using FTIR data from 2013 to 2019 was performed to derive background values of CO.

2.2 Numerical modelling

2.2.1 Copernicus CAMS EAC4

Total, black carbon (BC), organic matter (OM), dust (DU), sulfate (SU), and sea salt (SS) AOD_{550} were retrieved from the Copernicus Atmosphere Monitoring Service (CAMS) European Centre for Medium-range Weather Forecast (ECMWF) Atmospheric Composition Reanalysis 4 (EAC4) (Benedetti et al., 2009; Mangold et al., 2011; Morcrette et al., 2009). CAMS was selected for this study given its demonstrated ability to accurately reproduce AOD across various aerosol types (Chazette, 2026). Data can be downloaded from the official DOI: (Copernicus Atmosphere Monitoring Service, 2020,

https://doi.org/10.5194/egusphere-2026-3070
Preprint. Discussion started: 3 July 2026

https://ads.atmosphere.copernicus.eu/datasets/cams-global-reanalysis-eac4?tab=download, last access April 29th, 2025). Concerning the naturally emitted aerosols (dust and sea-salt), their sources are linked to prognostic and diagnostic model variables on the surface and near-surface. However, sources of anthropogenic aerosols (organic matter, black carbon and sulfate) originate from the MACCity anthropogenic emission inventory (based on the ACCMIP historical emissions extended to 2020 following RCP 8.5), while biomass burning emissions of BC and OM are provided by the Global Fire Assimilation System version 1.2 (GFASv1.2) (Inness et al., 2019). We extracted one month of data produced by CAMS EAC4 from September 1st, 2017, until October 1st, 2017, with a spatial resolution of 0.75°x0.75°, and a temporal resolution of 3h. We averaged the data around Reunion Island using a 1° radius box centered on Reunion Island.

2.2.3 ECMWF ERA5

ERA5 reanalysis is the fifth generation of ECMWF global reanalysis. This widely used product is comprehensively presented by Hersbach et al., 2020. In this work, the hourly pressure level outputs (37 levels) are used to plot synoptic maps with 0.25° x 0.25 ° resolution. The data can be accessed via the climate data store portal hosted by Copernicus (https://cds.climate.copernicus.eu/). Synoptic maps highlight the underlying atmospheric dynamics enabling long-range transport of aerosol.

2.2.2 FLEXPART

The long-range transport of wildfire CO from SA and Africa was simulated with the Lagrangian particle dispersion model FLEXPART version 10.4 (Pisso et al., 2019) in forward mode. The input emissions of CO into the model were adopted from the Copernicus Global Fire Assimilated System (GFAS) (Kaiser et al., 2012). In addition to emission fluxes of CO (and other pollutants), the product also provides estimates of the injection height of the wildfire plume, a feature that is crucial for accurate simulation of smoke dispersion. The model is driven by hourly reanalysis meteorological fields (ERA5) from ECMWF with 137 vertical levels (up to approximately 80 km) and a horizontal resolution of 0.5°×0.5° (Hersbach et al., 2020). FLEXPART, turbulence unresolved mesoscale motions (Stohl et al., 2005), and deep convection (Forster et al., 2007). The model output consists of 4-dimensional modelled concentrations extending from the surface up to 15 km height, wet and dry deposition variables. The FTIR a priori profiles and averaging kernel matrices were used to smooth CO vertical profiles over Reunion Island provided by FLEXPART using the following equation (Rodgers and Connor, 2003):

$$CO_{Flex\_smooth} = FTIR_{apriori} + Ak * (CO_{Flex} - FTIR_{apriori}), \quad (4)$$

where CO_{Flex_smooth} is the smoothed CO vertical profile from FLEXPART outputs, CO_{Flex} is the raw CO vertical profile provided by FLEXPART, $FTIR_{apriori}$ is the a priori profile from the FTIR, and Ak is the averaging kernel from the FTIR. Background values of CO derived from the FTIR 2013-2019 climatology were added to FLEXPART output profiles. The FTIR partial columns were compared to FLEXPART partial columns derived from vertical profiles to validate the injection height of wildfire plumes parametrized in the model.

https://doi.org/10.5194/egusphere-2026-3070
Preprint. Discussion started: 3 July 2026

3 Results

The results of this paper follow a multi-instrumental approach.

- The first step is to identify aerosol plumes by spotting high values of AOD over Reunion Island based on photometric measurements during the BB season. CAMS reanalyzes are then compared to our sun-photometer. Should this comparison prove consistent, CAMS aerosol chemical compound products can be used to identify the main specie responsible for these high values of AOD.
- The second step is to analyze the horizontal dispersion of AOD over the SWIO and the Southern Hemisphere using spaceborne observations from MODIS. CALIPSO is also exploited to identify aerosol layers and the species responsible in the vicinity of Reunion Island.
- Next, we identify aerosol plumes above Reunion Island during two episodes of high AOD values using ground-based lidars and assess their vertical distribution and optical characteristics. Specific characteristics of these plumes such as water vapor content are also studied.
- The last step is to assess the origin of these plumes and describe their preferred transportation routes based on FLEXPART modelling with CO as an air mass tracer. Comparison with ground based FTIR observations is performed to assess the validity of FLEXPART outputs.

3.1 Aerosol optical depths during September 2017

High AOD values were observed and modelled in September 2017 above Reunion Island. Figure 1 shows the AOD_{550} measured by the sun-photometer, as well as the total AOD_{550} and the contribution of various aerosol chemical compounds derived from CAMS EAC4 reanalysis.

https://doi.org/10.5194/egusphere-2026-3070
Preprint. Discussion started: 3 July 2026

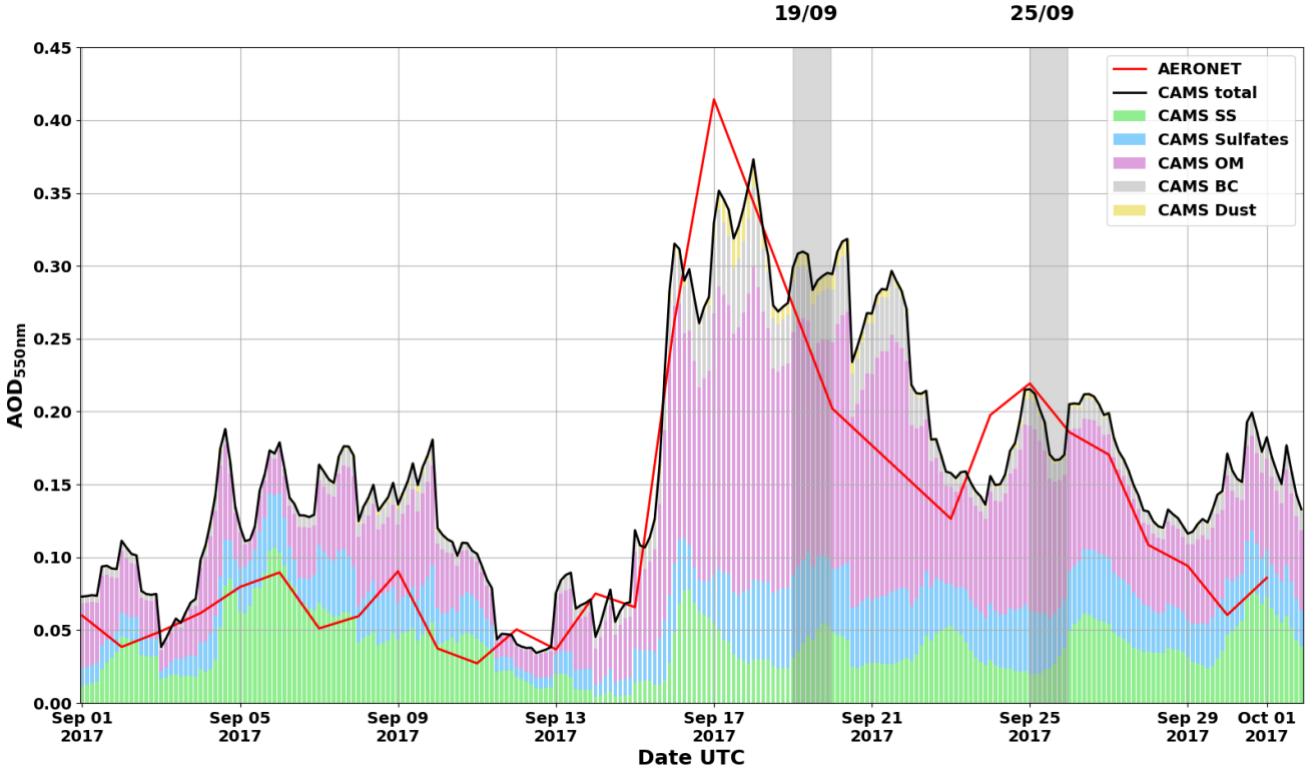

Figure 1: Daily total Aerosol optical depth AOD_{550} measured by a CIMEL sun-photometer (AERONET network) above Saint-Denis (red curve) during September 2017. Total and specific AOD_{550} produced with a 3h temporal resolution by CAMS EAC4: total AOD_{550} (black curve - CAMS total), AOD_{550} from black carbon (grey bars - CAMS BC), AOD_{550} from dust (yellow bars - CAMS Dust), AOD_{550} from sulfates (blue bars - CAMS Sulfates), AOD_{550} from organic matter (purple bars - CAMS OM), and AOD_{550} from sea-salt (green bars - CAMS other). Vertical areas in grey indicate two days of high AOD with concomitant lidar measurements: September 19th and 25th, 2017.

The usual AOD_{550} value from a monthly climatology encountered above Reunion Island in September is 0.09 ± 0.03 (Appendix A1, updated from(Duflot et al., 2022)). AOD_{550} from AERONET was particularly strong between September 16th and 23rd, 2017 (0.16-0.42), and between September 24th and 28th, 2017 (0.16-0.23). For those two periods, we selected concomitant lidar measurements (grey areas) on the 19th and 25th of September 2017. The high values observed in September 2017 are probably linked to the presence of BB plumes. In fact, a previous AOD_{440} climatology, variability and trend study from the same sun-photometer highlighted that sea-salt aerosols could be considered responsible for the AOD_{440} baseline, and BB plumes were responsible for the seasonal increase of AOD_{440} values during the BB season (Duflot et al., 2022). A good agreement can be observed between AERONET AOD_{550} and total AOD_{550} provided by CAMS, with a Spearman correlation coefficient of 0.901 ± 0.003 between the 11th and 28th of September 2017. One may observe increased differences between CAMS model and AERONET values between the 1st and the 11th of September. These differences could be due to the matrix averaging of CAMS values in a 1° radius box centered around Reunion Island. In fact, Reunion Island is surrounded by the Indian Ocean emitting sea-salt aerosols. Should the emissions of sea-salt be stronger above the ocean in this 1° radius box and during this specific

https://doi.org/10.5194/egusphere-2026-3070
Preprint. Discussion started: 3 July 2026

period, it would explain the bias between CAMS AOD and the Sun-photometer AOD. Concerning the different species contributing to the total AOD, organic matter (OM) contributes between 50 and 60 % to the high AOD_{550} values observed for the two periods previously described. Black carbon (BC), sulfates (SU) and sea-salt (SS) also contribute, but much less than OM (between 5 and 25%). Dust (DU) has a negligible contribution (less than 5%). Biomass burning emits many elements such as volatile and gaseous carbonaceous compounds (among which the carbon monoxide - CO), BC, and OC essentially made of degradation products from natural cellulose (Simoneit, 2002). The simultaneous rise in OM over Réunion Island, together with elevated AOD values, indicates a strong likelihood that BB smoke plumes are present above the site.

3.2.1 Passive remote sensing observations of AOD in the Southern Hemisphere

To assess the horizontal dispersion of these increased AOD values over Reunion Island, we used MODIS observations from AQUA and TERRA and compared average values of AOD from the first two weeks of September 2017 (Fig.2b), and the last two weeks of September 2017 (Fig.2c). We also added the cumulated FRP for the first two weeks of September 2017 (Fig.2a). During the first two weeks of September 2017, the cumulated FRP was particularly high above South America and Southern Africa, meaning that the BB activity was strong during this period. For the same period, strong AOD values were observed above Brazil, Namibia and Botswana (AOD >=1). The slight mismatch between the high FRP values and the high AOD values already highlights a dynamical transport occurring just after BB aerosol injection in the troposphere.

Two rivers of smoke could be described on figures 2b and 2c. One of them originated from Brazil, extended to the southeast over Bolivia, Argentina and Uruguay, before travelling over the Atlantic Ocean eastward, following a zonal route towards the western south African coast and the SWIO (Edwards et al., 2006; Flamant et al., 2022). The second one originated from Southern Africa, travelled to the Atlantic Namibian coastline, and extended from the northwest to the southeast over the Atlantic, before crossing South Africa and reaching the SWIO (Garstang et al., 1996; Swap et al., 2003). These dynamical processes are illustrated by the ERA5 horizontal wind average values at 600hPa (Fig.2b-c). Comparison between the two periods (Fig.2b-c) showed that higher values of AOD were observed over the SWIO for the second part of September. During this period, BB aerosol layers were suspected to travel above Reunion Island. BB aerosols were probably emitted by South America and Southern Africa between September 1st and 15th and followed one or the two rivers described previously before reaching the SWIO and Reunion Island between September 16th and 30th.

https://doi.org/10.5194/egusphere-2026-3070
Preprint. Discussion started: 3 July 2026

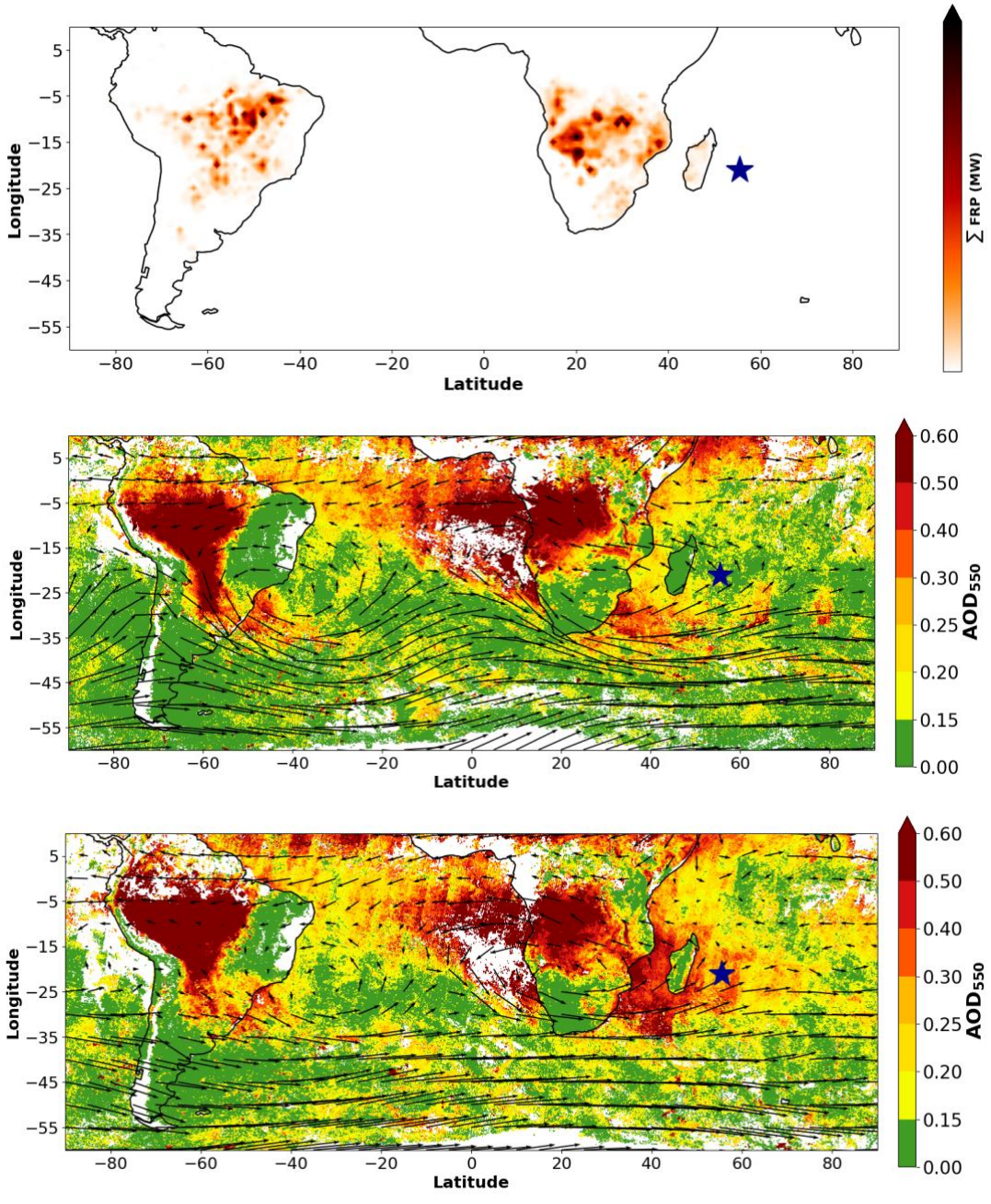

Figure 2: Cumulated FRP from MODIS AQUA (1° horizontal resolution) between September 1st and 15th (top). Averaged total Aerosol optical depth AOD_{550} derived from MODIS AQUA + TERRA between September 1st and 15th (middle), and between September 16th and 30th (low). The mean ERA5 wind fields at 600 hPa for each period have been added in black (middle-low). Reunion Island is represented by the blue star.

https://doi.org/10.5194/egusphere-2026-3070
Preprint. Discussion started: 3 July 2026

3.2.1 Active remote sensing observations of aerosol extinction in the Southern Hemisphere

Satellite products from CALIOP provided further information about the aerosol composition of the free troposphere in the SWIO (Fig. 3a-b). The two overpasses corresponded to the high AOD values observed by MODIS during the second half of September. They both showed vast smoke layers above the east coast of Southern Africa and Madagascar (Fig.3a). These expanded from 0 to -35 ° of latitude, and from 0 up to 9 km asl. Above the east coast of Southern Africa and Madagascar, the main aerosols identified were aerosols from continental pollution mixed with smoke and elevated smoke (Fig.3b). Above the ocean around Madagascar, two layers could be identified: the lowest were made of marine aerosols (0 up to 2 km asl), and the highest were made of elevated smoke (4 up to 9 km asl). These results enabled us to assess the vertical dispersion of aerosols in the vicinity of the SWIO.

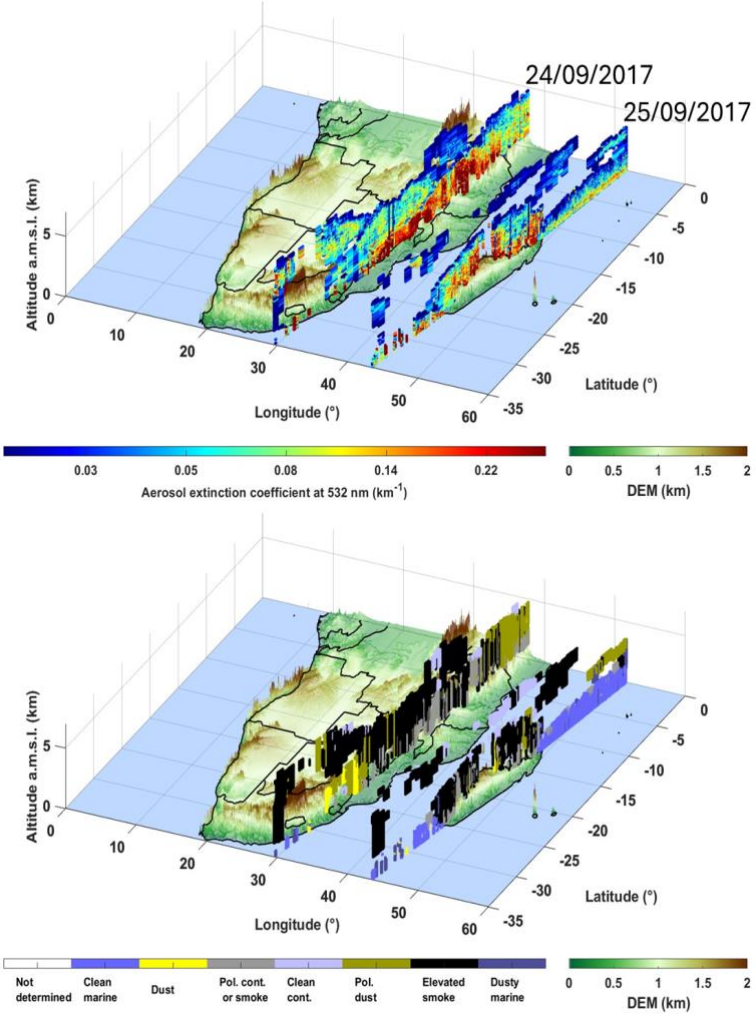

Figure 3: (a) Aerosol extinction coefficient at 532 nm derived from the space-borne lidar CALIOP. (b) Same as (a) but for CALIOP-derived aerosol typing. Four nighttime orbits appear in these plots: (i) two of them on September 24th, 2017, between 23:04 and

https://doi.org/10.5194/egusphere-2026-3070
Preprint. Discussion started: 3 July 2026

23:31 UTC over the east coast of Southern Africa, (ii) and two of them on September 25th, 2017, between 21:55 and 22:35 UTC over Madagascar.

These findings indicate that the elevated AOD values recorded by MODIS over the SWIO during the latter half of September were primarily driven by BB smoke, often combined with continental pollution and, in some cases, marine aerosols.

3.3 Vertical profiles of aerosol optical properties

Vertical profiles of aerosol extinction coefficient at 355 (α_{355}) and 532 nm (α_{532}), as well as the Ångström exponent ($Ä_{355/532}$) were derived from lidar measurements on the 19th and 25th of September 2017.

On September 19th, 2017, the total AOD values at 355 and 532 nm measured by sun-photometer were respectively 0.34 and 0.21. The ground based lidars captured an aerosol plume in the low troposphere between 2.8 and 4.7 km asl (Fig.4). The AOD values at 355 and 532 nm of this plume derived from the lidar measurements were respectively 0.19 and 0.14, lower than the sun-photometer AOD values. The discrepancies observed between lidar and sun-photometer AOD values can be explained by the optical geometry of our lidar instruments (overlap factors, see (Gantois et al., 2024)), the difference in elevation between the sun-photometer site (80 m asl) and the lidars site (2160 m asl), and the presence of aerosols in the boundary layer. Based on lidars measurements, the September 19th plume was characterized by an $Ä_{355/532}$ of 1.32 ± 0.23. The usual values of Ä for BB aerosols can vary between 2.2 for fresh plumes and 1.2 for aged plumes (Reid et al., 1998) and sometimes even reach very low values for very old plumes (0.06, (Wandinger, et al., 2002)). In fact, it has been described that particles grow in size during the ageing of BB plumes (Fiebig et al., 2003). The Raman signals bellow 5 km were too poor for the two wavelengths, which prevented us from determining an LR profile for this plume.

https://doi.org/10.5194/egusphere-2026-3070
Preprint. Discussion started: 3 July 2026

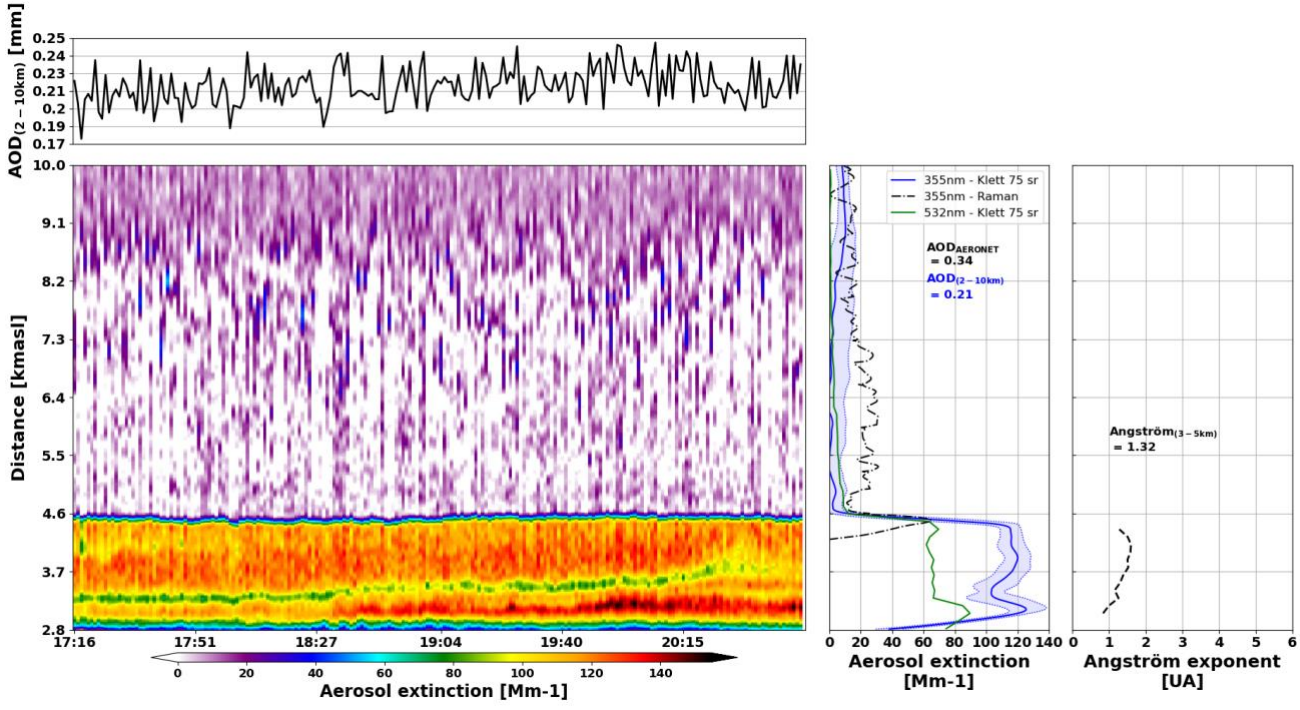

Figure 4: ***[left]*** **Aerosol extinction time-height cross-section over Maïdo facility (Reunion Island) on September 19th, 2017.** ***[center]*** **Mean vertical profile of aerosol extinction from Klett inversion at 355 nm (blue curve: Li1200, LR = 75 sr) and corresponding standard deviation (shaded blue), 532nm (green curve: LiO3T, LR = 75 sr), and from Raman inversion at 387 nm (black dotted curve: Li1200). AOD between 2 and 10 km (blue) is obtained from the Li1200 retrieval, and total AOD (black) from AERONET sun photometer.** ***[right]*** **Ångström exponent (black dotted line) vertical profile.**

On September 25th, 2017, the total AOD values at 355 and 532 nm measured by sun-photometer were respectively 0.37 and 0.23. Ground based lidars captured two aerosol plumes in the low troposphere between 3.3 and 5 km asl, and in the middle troposphere between 5 and 9 km (Fig.5). The specific AOD values at 355 and 532 nm for both plumes derived from lidar measurements were respectively 0.12 and 0.07 for the lowest, and 0.17 and 0.09 for the highest. Again, the sum of these AODs (0.29 and 0.16) is lower than the total AOD measured by AERONET, most probably due to the overlap factors of our instruments and the presence of aerosols in the 0-2.5km layer. A mean LR of 75 ± 9 sr at 355 nm was determined from Raman inversion for the highest plume, consistent with BB aerosols (Wandinger, et al., 2002). This LR value was used to reprocess data for both days of measurements to increase comparability, and for both wavelengths, as this value of LR for 532 nm is consistent with previously published studies (Haarig et al., 2018). The highest plume was characterized with higher values of $Ä_{355/532}$ than the lowest plume (1.60 ± 0.06 vs 1.45 ± 0.12, respectively). This is consistent with, but does not uniquely demonstrate, the presence of a distinct aerosol population potentially associated with fresher smoke (Fiebig et al., 2003).

https://doi.org/10.5194/egusphere-2026-3070
Preprint. Discussion started: 3 July 2026

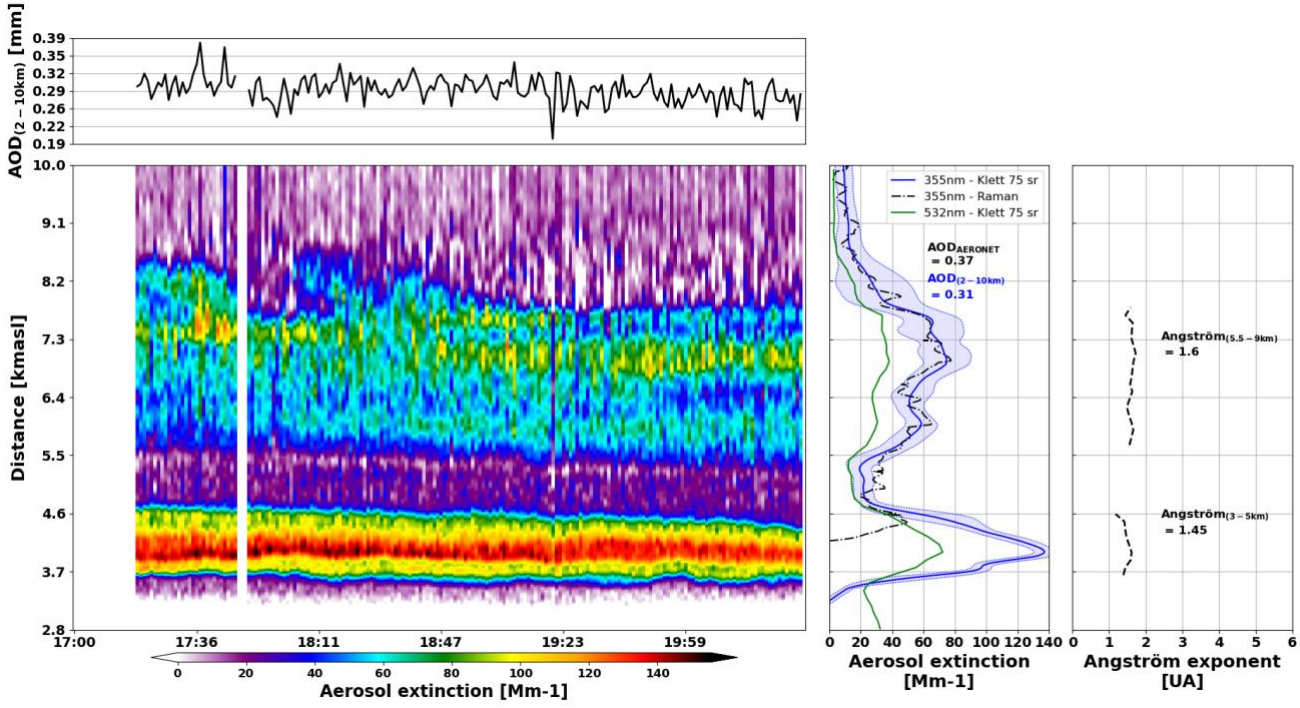

Figure 5: ***[left]*** **Aerosol extinction time-height cross-section over Maïdo facility (Reunion Island) on September 25th, 2017.** ***[center]*** **Mean vertical profile of aerosol extinction from Klett inversion at 355 nm (blue curve: Li1200, LR = 75 sr) and corresponding standard deviation (shaded blue), 532nm (green curve: LiO3T, LR = 75 sr), and from Raman inversion at 387 nm (black dotted curve: Li1200). AOD between 2 and 10 km (blue) is obtained from the Li1200 retrieval, and total AOD (black) from AERONET sun photometer.** ***[right]*** **Ångström exponent (black dotted line). Corresponding mean values are given for each aerosol layer.**

3.4 Water vapor content

Vertical profiles of WVMR were retrieved from the 387 nm and 407 nm channels of the Li1200. On September 19th, 2017, time-series of WVMR vertical profiles (Fig.6) showed high quantities of water vapor inside the aerosol layer (2.08 ± 0.21 g.kg^{-1}). A high uncertainty (1.54 g.kg^{-1}) in the WVMR measurement precision concerning this aerosol layer was estimated (almost 74% of the mean WVMR). This layer was also characterized by high precipitable water values with lower values during the first hour of measurement (2.75 ± 0.04 mm), and higher values for the rest of the night (3.00 ± 0.08 mm). This would suggest that the layer content was variable over time. In fact, AOD values slowly increased during the night which could be consistent with aerosol advection in this layer. However, there was little scattering of WVMR around the mean, as supported by the low standard deviation value (less than 10% of the mean WVMR).

https://doi.org/10.5194/egusphere-2026-3070
Preprint. Discussion started: 3 July 2026

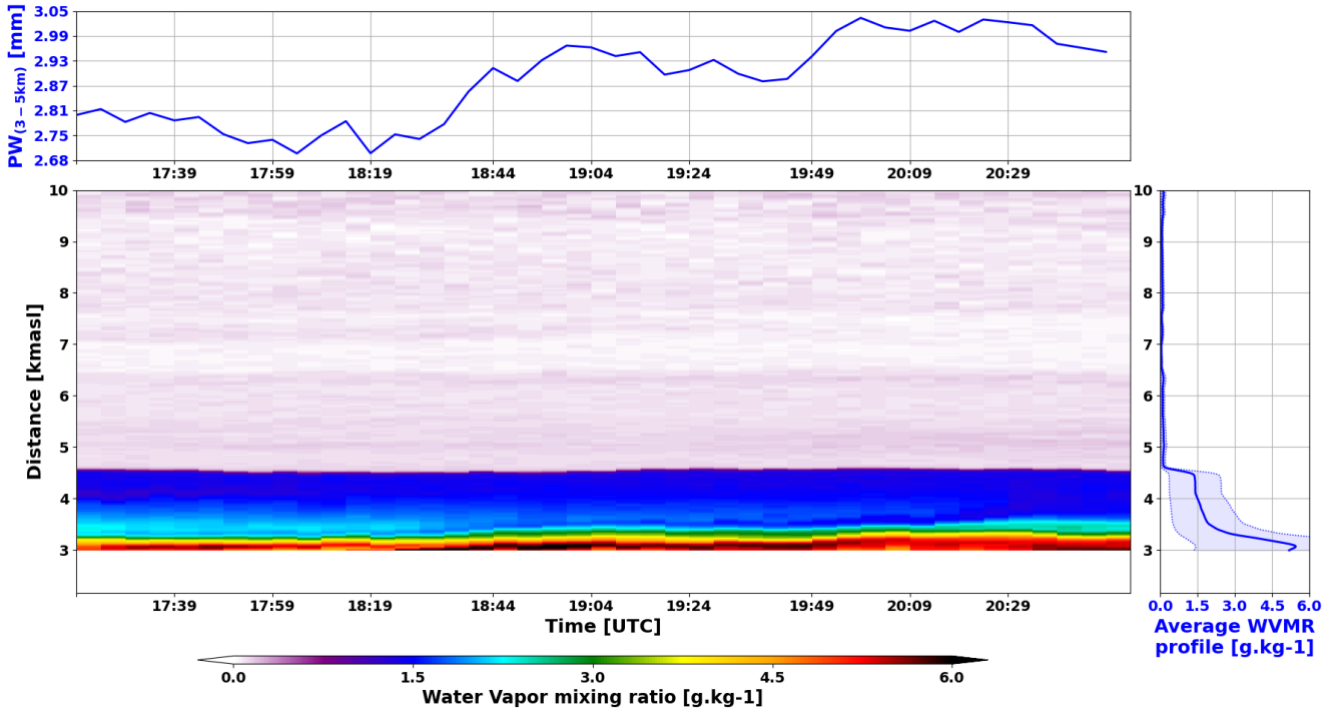

Figure 6: ***[Bottom left]*** **Water Vapor Mixing Ratio (WVMR) vertical profiles over Maïdo facility (Reunion Island) on September 19th, 2017.** ***[Top left]*** **Precipitable Water (PW) values (blue curve), and AOD values (black curve) between 3 and 5 km over Maïdo facility (Reunion Island) on September 19th, 2017.** ***[Bottom right]*** **Mean WVMR vertical profile over Maïdo facility (Reunion Island) on September 19th, 2017, with uncertainty in shaded blue.**

The scatter plot between WVMR and aerosol extinction values (Fig.7) highlighted the structure of this layer with a bottom layer enriched with water vapor and slowly drying up with the altitude, a mid-layer with stable values of WVMR, and a top layer quickly drying up with the altitude. In the bottom layer, the extinction values were stable, but the WVMR decreased quickly, which means that the aerosol content and the WVMR are decoupled. In the middle layer, both the aerosol content and the WVMR were stable. In the top layer, the extinction and the WVMR values decreased, similarly.

https://doi.org/10.5194/egusphere-2026-3070
Preprint. Discussion started: 3 July 2026

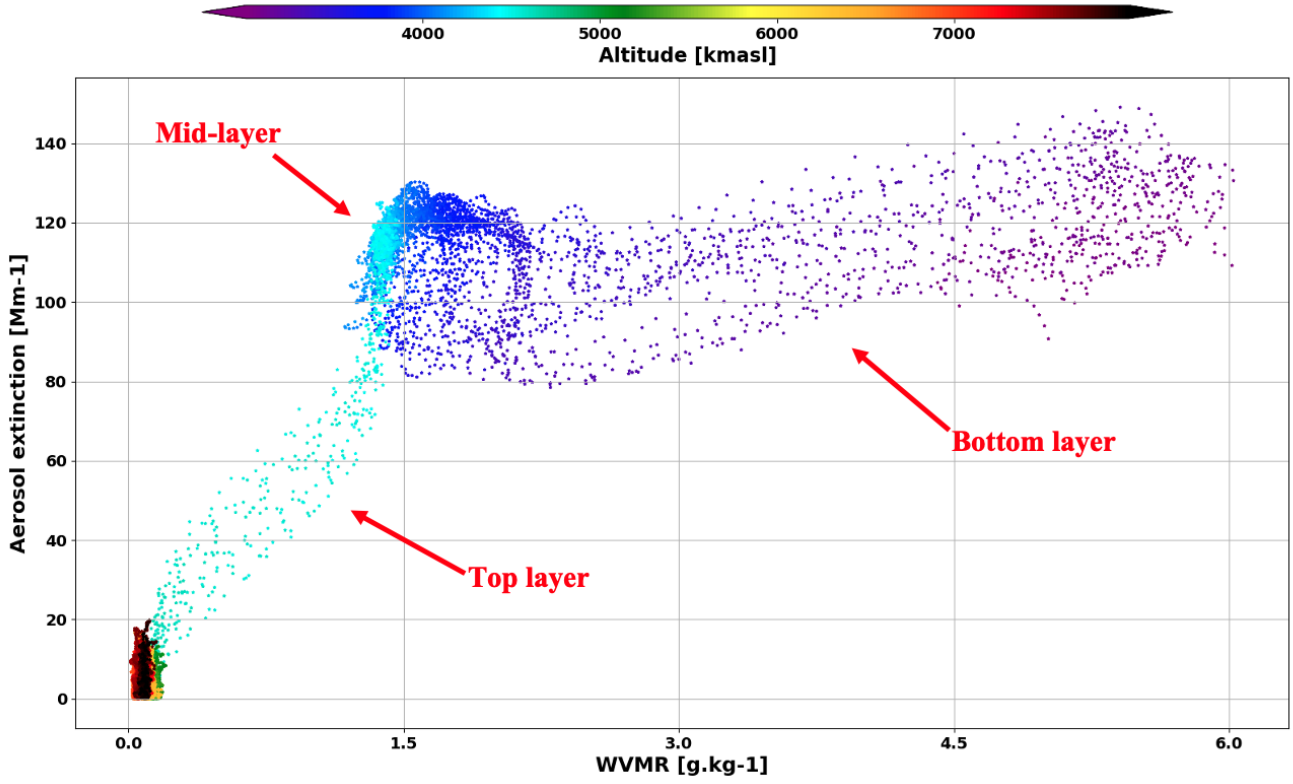

Figure 7: Scatter plot of Aerosol extinction and WVMR as a function of altitude derived from lidar measurements over Maïdo facility (Reunion Island) on September 19th, 2017.

On September 25th, 2017, time-series of WVMR vertical profiles (Fig.8) showed differences in water vapor content between the highest and the lowest aerosol layers. The highest layer was the driest (0.09 ± 0.04 $g.kg^{-1}$), when the lowest layer had the largest quantities of water vapor (1.27 ± 0.22 $g.kg^{-1}$). A high uncertainty (0.94 $g.kg^{-1}$) in the WVMR measurement precision concerning the lowest aerosol layer was estimated (almost 74% of the mean WVMR). This layer was also characterized by slowly decreasing, yet high precipitable water values with higher values during the first two hours of measurement (2.72 ± 0.06 mm), and lower values for the rest of the night (2.39 ± 0.15 mm). Again, this suggests that the layer content is variable over time. However, there was little scattering of WVMR around the mean, as supported by the low standard deviation value (almost 17% of the mean WVMR). AOD values remained rather stable during the night (0.12 ± 0.006) which is not in favor of any advection or loss of aerosols over time.

https://doi.org/10.5194/egusphere-2026-3070
Preprint. Discussion started: 3 July 2026

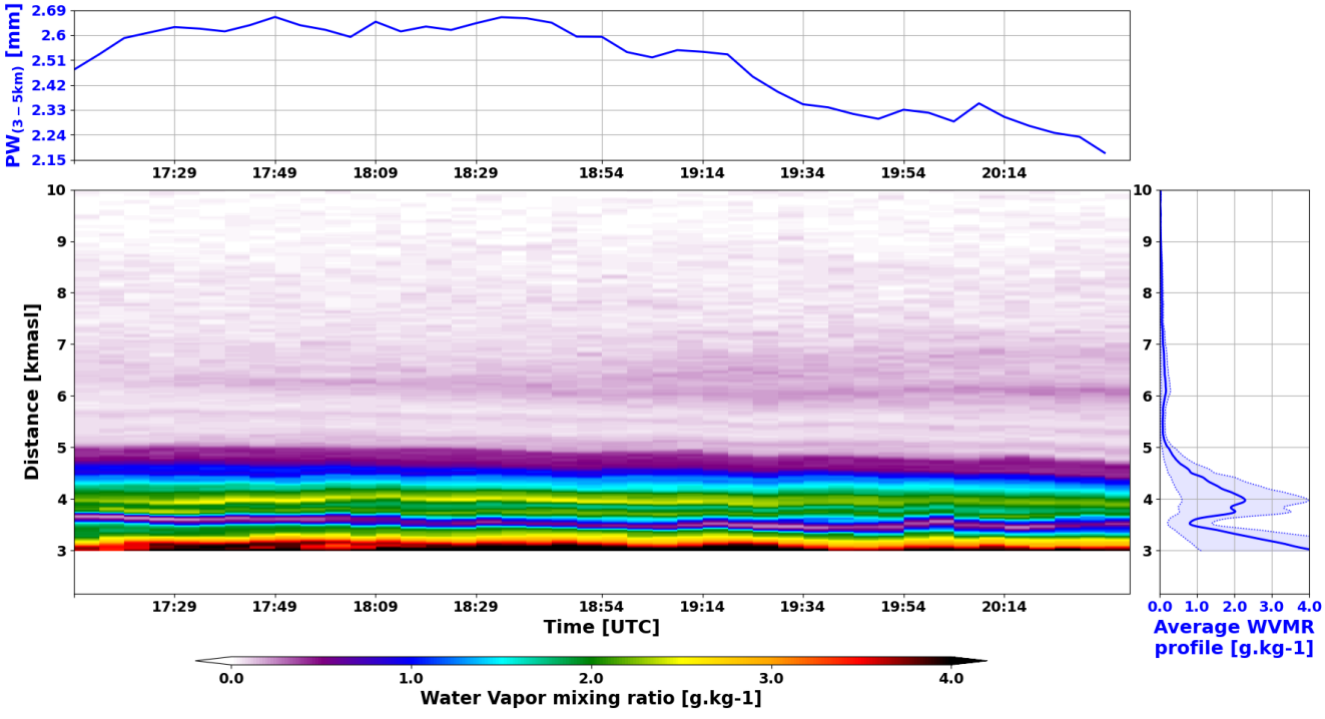

Figure 8: ***[Bottom left]*** **Water Vapor Mixing Ratio (WVMR) vertical profiles over Maïdo facility (Reunion Island) on September 25th, 2017.** ***[Top left]*** **Precipitable Water (PW) values (blue curve), and AOD values (black curve) between 3 and 5 km over Maïdo facility (Reunion Island) on September 25th, 2017.** ***[Bottom right]*** **Mean WVMR vertical profile over Maïdo facility (Reunion Island) on September 25th, 2017, with uncertainty in shaded blue.**

The scatter plot between WVMR and aerosol extinction values (Fig.9) revealed different structures: **(i)** between 3 and 3.5km the atmosphere was wet but aerosol-free, **(ii)** the lowest aerosol layer between 3.5 and 5 km was wet and its water vapor content increased up to 4 km and then decreased exponentially, and **(iii)** the highest aerosol layer between 5.5 and 8.5km was dry. A simultaneous monotonic increase of the particle backscatter coefficient and the RH was observed between 4 and 4.5 km. The variations of WVMR and potential temperature were respectively 1.36 $g.kg^{-1}$ and 1.88 K between those two layers.

https://doi.org/10.5194/egusphere-2026-3070
Preprint. Discussion started: 3 July 2026

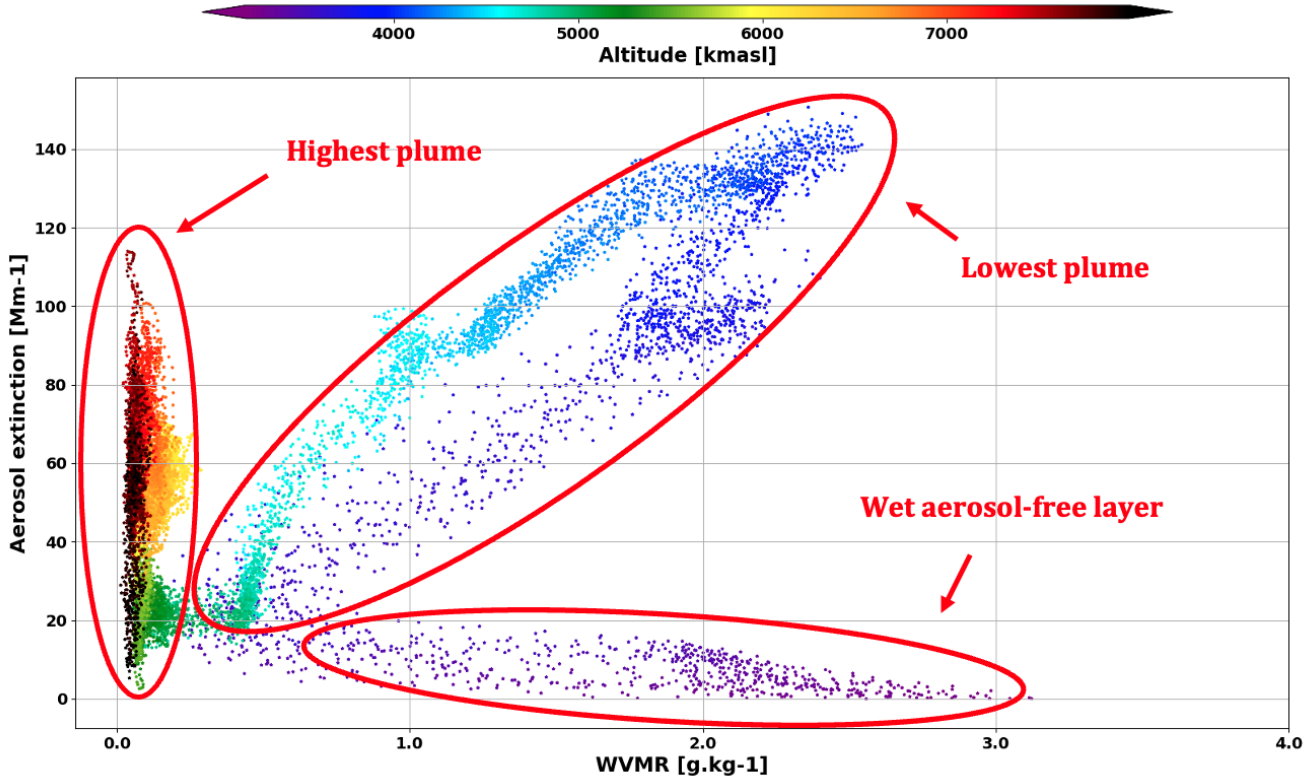

Figure 9: Scatter plot of Aerosol extinction and WVMR as a function of altitude derived from lidar measurements over Maïdo facility (Reunion Island) on September 25th, 2017.

3.5 Source regions

To investigate the origin of the observed plumes and explain the dynamical processes involved we used FLEXPART modelling products. CO as a passive air mass tracer was simulated forward from the biomass burning source. FLEXPART simulations were quantitatively validated using FTIR measurements performed at Maïdo.

Time-series of CO concentration vertical profile and CO total column in 2017 measured by Maïdo FTIR (Fig. 10) showed an increase of CO with a mean value of $(1.34 \pm 0.26) *10^{18}$ molecules.cm^2 between July and November (BB season) and between 2.5 and 12.3 km (essentially middle and low troposphere). This value is higher than the corresponding climatology value of $(1.15 \pm 0.18) *10^{18}$ molecules.cm^2 computed from FTIR measurements between 2013 and 2019. This is consistent with the presence of BB plumes during this period (Duflot et al., 2010).

Both the CO total column time-series derived from FTIR measurements and the AOD values recorded by AERONET indicate that the BB season starts in July. The discrepancies observed between January and May can be attributed to the difference in instrument elevation: the FTIR site is located at 2160 m asl, placing it above the boundary layer at night, while the sun-photometer operates at 80 m asl, where it is influenced by the urban pollution within the boundary layer.

https://doi.org/10.5194/egusphere-2026-3070
Preprint. Discussion started: 3 July 2026

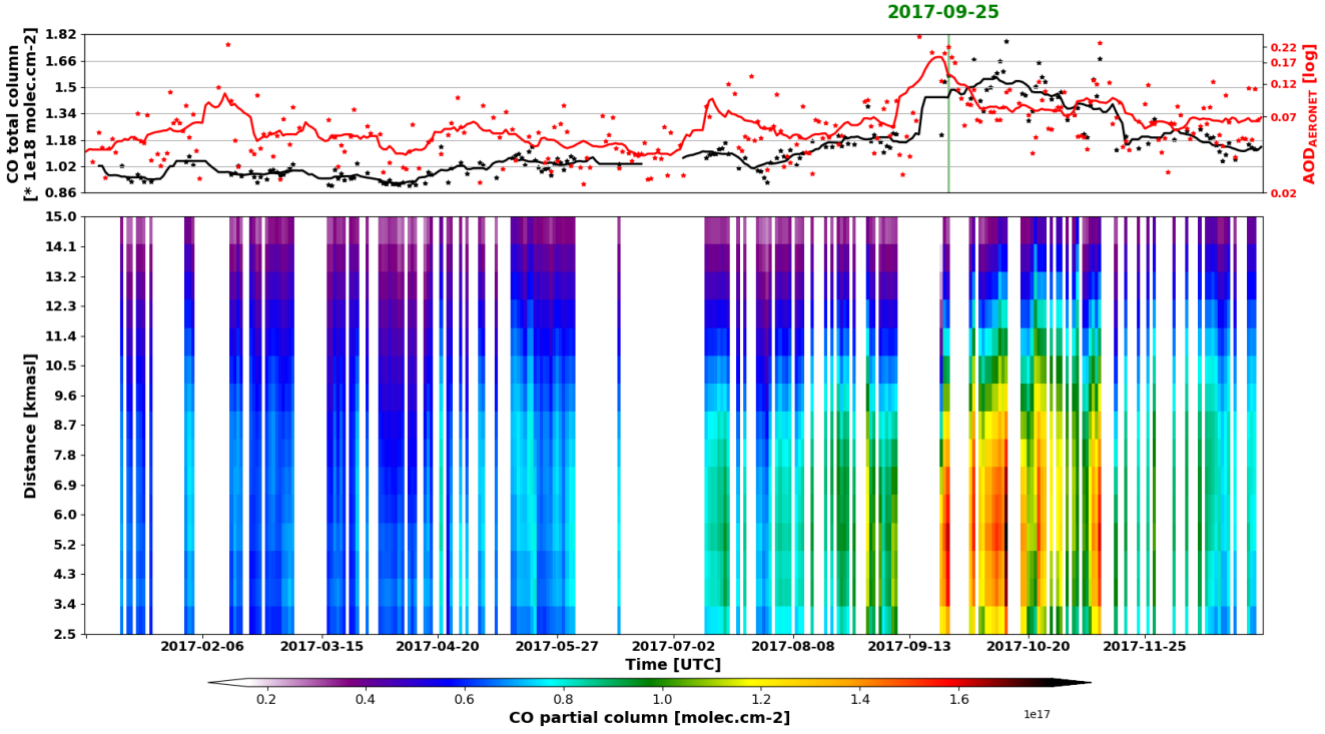

Figure 10: *[Bottom]* Time-series of CO partial columns bounded by the altitude on the vertical axis between 2.5 and 15 km measured by the FTIR over Maïdo observatory during year 2017. *[Top]* Time-series of CO partial column between 2.5 and 15 km measured by the FTIR (black stars), and total AOD values from AERONET (red stars) during year 2017 with their respective 15-days moving average (plain lines).

The comparison between FLEXPART simulation outputs and FTIR measurements for CO partial columns between 2 and 15 km from August the 1st, 2017 to November the 1st, 2017 is represented in Figure 11. A smoothing was applied to each FEXPART profiles, using the FTIR averaging kernels and the a priori profiles as described in the methodology section. CO concentration varied between $9.8*10^{17}$ and $1.8*10^{18}$ molecules.cm^{-2} for FLEXPART output and the FTIR with a mean of $9.5*10^{17}$ and $1.9*10^{18}$ molecules.cm^{-2}, respectively. The correlation coefficient between the measured and simulated CO partial columns between 2 and 12 km was 0.82.

https://doi.org/10.5194/egusphere-2026-3070
Preprint. Discussion started: 3 July 2026

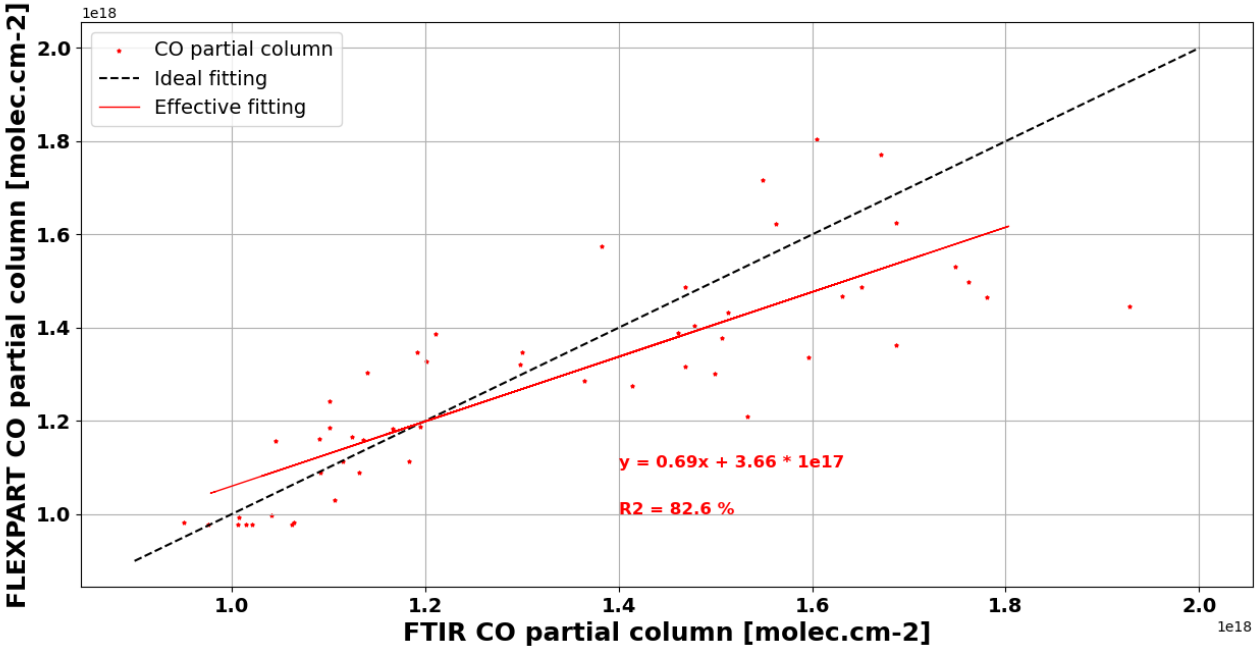

Figure 11: Comparison between FLEXPART simulation outputs smoothed by FTIR averaging kernels and FTIR measurements for daily averaged CO partial columns between 2.16 and 15 km. The red line represents the theoretical linear regression. Background climatology values of CO partial columns from the FTIR were added to FLEXPART partial columns.

The only concomitant measurement between the FTIR and FEXPART for our case study was on September 25th, 2017. The corresponding FLEXPART and FTIR vertical profiles of CO concentration are visualized on Figure 12. A smoothing was applied to the FLEXPART profile, using the FTIR averaging kernel and the a priori profile as described in the methodology section. After adding the background value of CO derived from the FTIR climatology to the FLEXPART partial columns, we found matching values between the FLEXPART and FTIR partial columns from 2.16 to 5 km ($6.16*10^{17}$ vs $6.11*10^{17}$ molecules.m^{-2}, respectively), 5 to 15 km ($1.15*10^{18}$ vs $1.02*10^{18}$ molecules.m^{-2}, respectively), and 2.16 to 15 km ($1.62*10^{17}$ vs $1.49*10^{17}$ molecules.m^{-2}, respectively).

The good agreement between simulated and measured CO profiles gives confidence in our simulations. Comparison between FLEXPART CO partial columns (Fig. 12) and lidar aerosol extinction profiles (Fig. 4 and 5) shows a very good agreement in terms of aerosol layer altitudes. On September 19th, the single aerosol plume detected by lidar instruments between 2.8 and 4.7 km asl corresponds well to the CO-enriched layer simulated by FLEXPART in terms of altitude range. On September 25th, the two distinct aerosol layers identified by lidar instruments (between 3.3 and 5 km and between 5 and 9 km asl) are also consistently simulated by FLEXPART. This agreement in layer altitude between these two approaches provides a qualitative validation of the FLEXPART simulations by lidar observations and confirms that the transport model correctly reproduces the vertical structure of the BB plumes reaching Reunion Island.

https://doi.org/10.5194/egusphere-2026-3070
Preprint. Discussion started: 3 July 2026

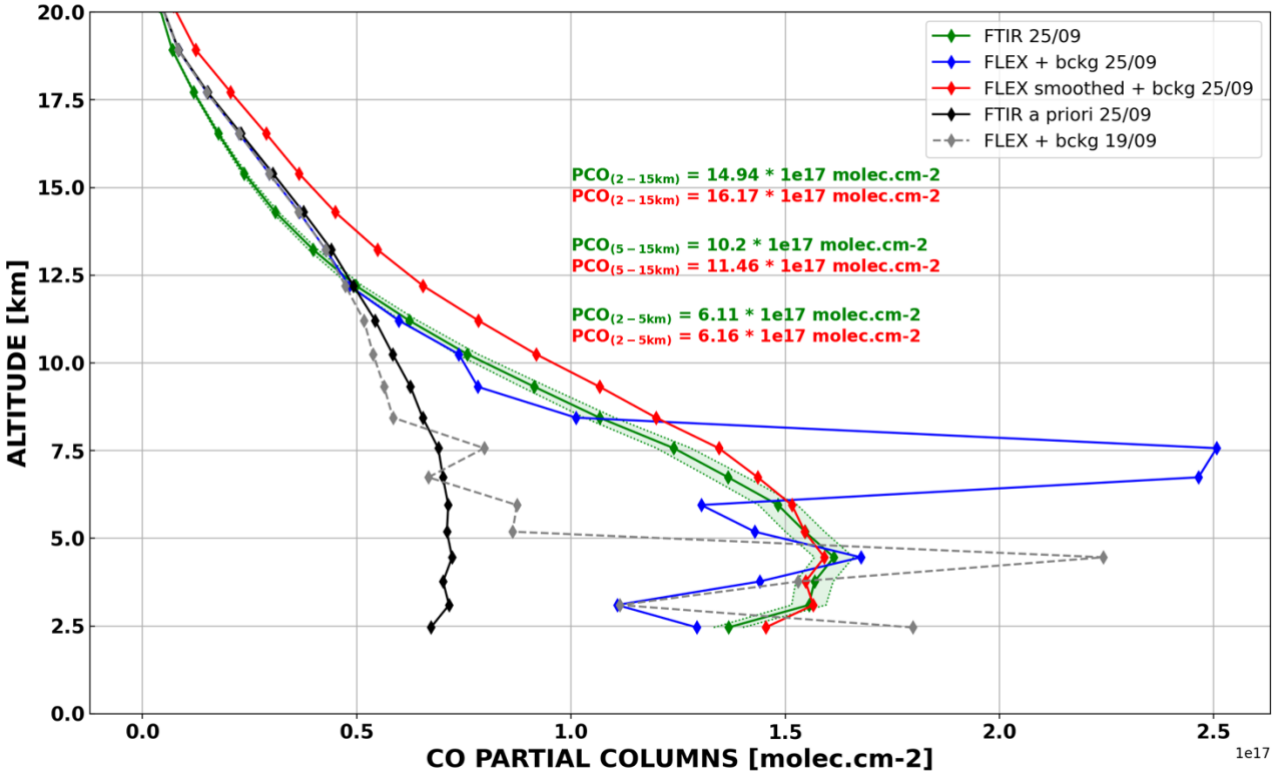

Figure 12: Vertical profile of CO partial columns over Maïdo observatory on September 25th, 2017, from FLEXPART forward mode before (Blue curve) and after (Red curve) smoothing using the FTIR averaging kernel and a priori profile (Black curve). Vertical profile of CO partial columns over Maïdo observatory on September 25th, 2017, from FTIR measurement (green curve) with the associated uncertainty in shaded green. FLEXPART vertical profile of CO partial columns over Maïdo observatory on September 19th, 2017, without smoothing (no FTIR data available).

To better understand the dynamical processes involved and visualize the atmospheric transport patterns, FLEXPART was run in forward mode with CO from BB as a tracer, emitted from South America and Southern Africa during two different simulations. Results can be visualized in the supplementary video (Gantois, 2026) showing the concentration of CO emitted by wildfires from each continent and integrated along the altitude vector, as well as the corresponding vertical profile of CO concentration over Reunion Island between September 16th and 26th, 2017.

The transport regimes identified with FLEXPART simulations (Fig.13 and 14) are coherent with the aerosol optical properties profiles retrieved from lidar measurements and align with the dynamical processes described in several studies (Flamant et al., 2022; Ranaivombola et al., 2023), such as the importance of vertical injection, stratified transport, and recirculation of Southern African BB plumes over the SWIO.

On September 19th, 2017 (Fig.13), FLEXPART indicates that the plume observed between 2.8 and 4.7 km is largely dominated by Southern African BB emissions (>88 %). The Ångström exponent derived from lidar measurements ($Ä_{355/532}$ = 1.32 ± 0.23) is characteristic of moderately aged BB aerosol, indicating that the plume could have undergone some microphysical

https://doi.org/10.5194/egusphere-2026-3070
Preprint. Discussion started: 3 July 2026

evolution during transport. The vertical coherence of the extinction profiles and the limited variability of the Ångström exponent within this layer suggest low mixing, consistent with transport within a stratified lower tropospheric flow. This behavior matches observations from AEROCLO-sA (Flamant et al., 2022), who showed that Southern African smoke can remain confined within well-defined lower tropospheric layers during export, especially under the influence of anticyclonic circulation. This recirculation mechanism has also been highlighted by (Ranaivombola et al., 2025), who demonstrated that BB aerosols can accumulate over South Africa before being advected eastward towards the SWIO and Reunion Island. FLEXPART results for this case are therefore in accordance with a regional recirculation, followed by a direct export route.

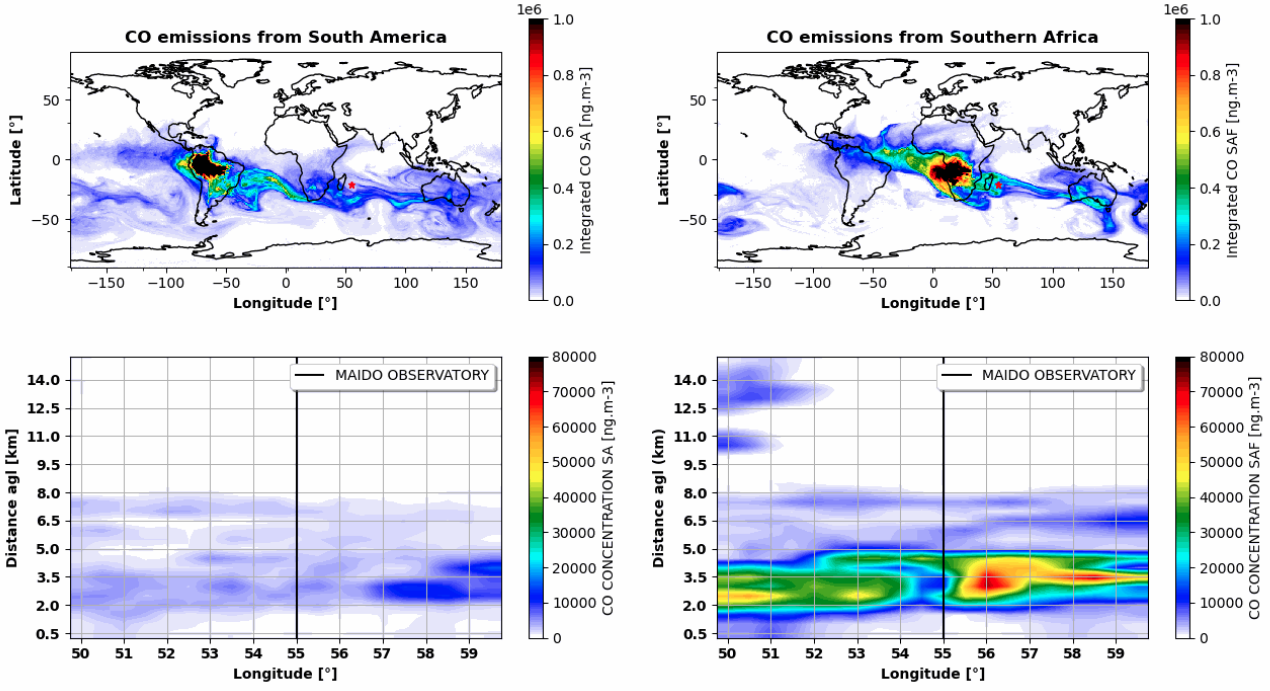

Figure 13: FLEXPART partial column CO emitted from biomass burning in South America *[left]* and Southern Africa *[right]* integrated between 0 and 15 km *[top]*, and vertical profiles at the latitude of 21.1°S Maido observatory, the longitude location of the Maido observatory shown as a black line*[bottom]* on September 19th, 2017, at 18h UTC.

On September 25th, 2017 (Fig.14), FLEXPART reveals two vertically separated plumes with distinct source contributions and optical signatures, suggesting different dynamical processes.

The upper plume (between 5 and 9 km) is dominated by Southern African emissions (> 70%) and shows a higher Ångström exponent ($Ä_{355/532}$ = 1.60 ± 0.06). This is consistent with, but does not uniquely demonstrate, the presence of a distinct aerosol population potentially associated with fresher smoke. This supports the hypothesis of rapid vertical injection up to the middle troposphere, potentially associated with convective uplift over Southern Africa. Such elevated and vertically decoupled smoke layers are consistent with observations reported by (Flamant et al., 2022), who documented the frequent presence of BB aerosol above 5 km and emphasized the role of large scale uplift and convective processes in their formation and long-range transport.

https://doi.org/10.5194/egusphere-2026-3070
Preprint. Discussion started: 3 July 2026

In contrast, the lowest plume (between 3.3 and 5 km) is characterized by a lower Ångström exponent ($Ä_{355/532}$ = 1.45 ± 0.12), indicating more aged and/or mixed aerosols. FLEXPART attributes this layer to combined contributions from Southern Africa and South America, which is consistent with large scale circulation patterns described in the literature. Long-range transport of South American BB emissions across the Atlantic has been widely documented (Duflot et al., 2010; Edwards et al., 2006), with air masses interacting with Southern African outflow before reaching the SWIO. This type of intercontinental mixing in the lower troposphere is consistent with previous studies showing that aerosol variability over Reunion Island is influenced by both regional BB and long-range transport processes (Duflot et al., 2010; Ranaivombola et al., 2023, 2025). This complexity reflects the influence of multiple transport pathways and synoptic scale circulations, leading to vertically structured aerosol layers with distinct content compositions (Flamant et al., 2022). This interpretation is further supported by AEROCLO-sA observations over the Namibian coast, which highlight strong variability and mixing of air masses in the lower troposphere driven by mesoscale and large scale processes (Chazette et al., 2019).

The quantitative difference in Ångström exponent between the two plumes confirms that they correspond to distinct aerosol populations with different aging states and transport histories, rather than a single vertically continuous plume. This vertical decoupling reflects the coexistence of: **(i)** a freshly uplifted Southern African smoke plume in the middle troposphere, driven by convective injection processes, and **(ii)** a mixed aged smoke plume in the lower troposphere, resulting from both long-range transport and recirculation.

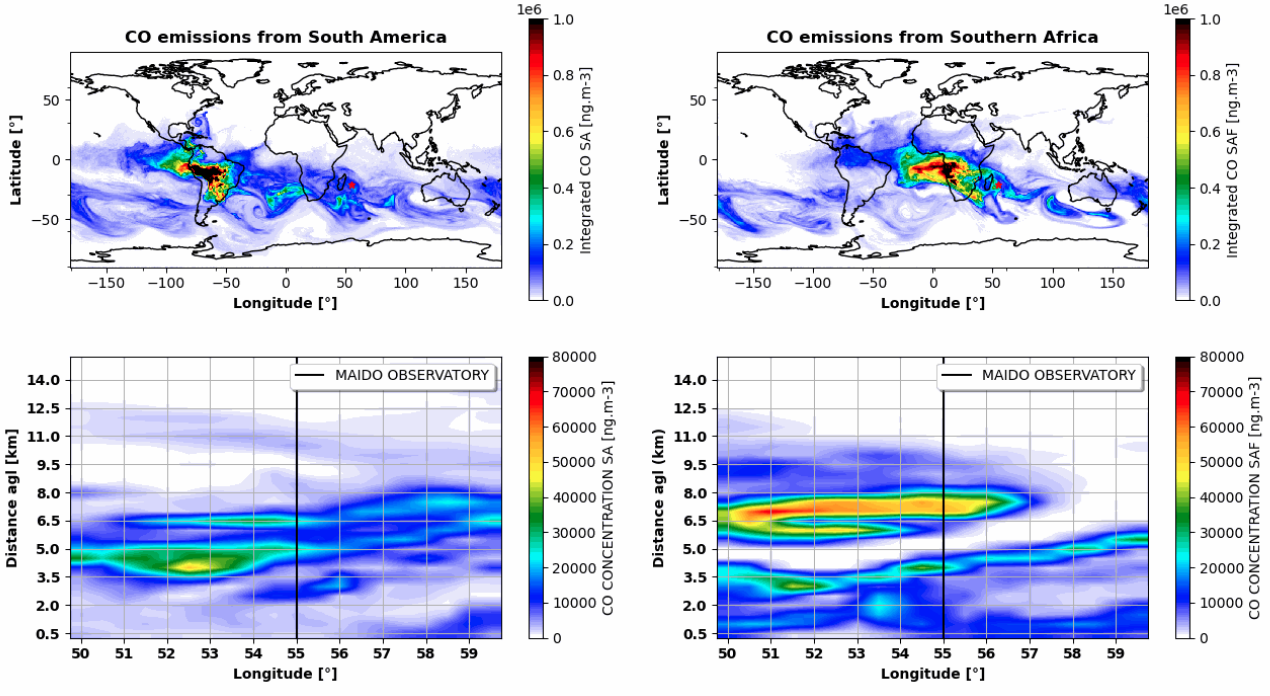

Figure 14: same as Fig 13, but for September 25th, 2017, at 18h UTC.

https://doi.org/10.5194/egusphere-2026-3070
Preprint. Discussion started: 3 July 2026

These results support the fact that the SWIO atmosphere is under the influence of a multi-source transport system where the vertical distribution of aerosol optical properties depends on vertical injection mechanisms and large-scale circulations.

4 Discussion and summary

This study investigated BB aerosol transport over Reunion Island during September 2017 using a multi-instrumental approach combining ground-based observations, satellite products, and numerical modelling. AOD_{550} over Reunion Island from AERONET measurements was unusually high (0.16-0.42) during the second half of September, well above the monthly climatological value of 0.09 ± 0.03. Chemical apportionment from CAMS EAC4 reanalysis (validated against AERONET, r = 0.90) indicated that organic matter was the dominant contributor (50-60 %), supporting attribution to BB emissions. Satellite observations revealed extensive smoke export from Southern Africa and South America towards the SWIO, resulting in vertically stratified elevated smoke layers in the low and middle troposphere of the basin's western region. Ground-based lidar observations in Reunion provided high-resolution vertically resolved aerosol optical properties on two specific days. FLEXPART simulations, validated using FTIR CO observations (r = 0.82), reproduced the observed variability and identified source regions and transport pathways. On September 19th, a single aerosol layer of Southern African origin was observed between 2.8 and 4.7 km, with an Ångström exponent of 1.32 ± 0.23, consistent with moderately aged BB particles. On September 25th, two vertically decoupled layers were identified: a lower layer (3.3-5 km, Å = 1.45 ± 0.12) with mixed aged aerosols from Southern Africa and South America, and an upper, drier layer (5-9 km, Å = 1.60 ± 0.06) dominated by fresher Southern African emissions consistent with rapid convective uplift into the mid-troposphere. Water vapor profiles confirmed the vertical decoupling, with moist conditions in the lower layer and very dry conditions in the upper one.

These vertically resolved observations reveal that aerosol variability over Reunion Island during the BB season cannot be fully understood through column-integrated measurements alone. The coexistence of two vertically decoupled layers on September 25th with distinct optical properties, moisture content, and origins, reveals that the SWIO free troposphere acts as a convergence zone for aerosol transport pathways operating at different vertical levels and timescales. The lower layer, relatively older and more humid layer results from mixing of BB aerosols from recirculating Southern African plumes and South American outflows through intercontinental transport in the lower troposphere. The upper layer, relatively fresher and drier, is consistent with rapid convective uplift of BB aerosols over Southern Africa into the mid-troposphere followed by fast zonal export. These findings highlight the role of synoptic-scale processes, including uplift, recirculation, and long-range transport, in producing vertically structured aerosol layers over the SWIO.

Our results are consistent with the current literature. The lidar ratio retrieved from Raman inversion for the upper layer on September 25th (75 ± 9 sr at 355 nm) and the observed Ångström exponents (1.32-1.60) are both consistent with values established for moderately aged BB smoke in the DeLiAn reference dataset (Floutsi et al., 2023). The ORACLES airborne

https://doi.org/10.5194/egusphere-2026-3070
Preprint. Discussion started: 3 July 2026

campaign (Redemann et al., 2021) over the southeast Atlantic documented vertically structured smoke layers from Southern Africa, with multi-layered plumes exhibiting vertical variability in optical properties linked to aerosol ageing, notably a loss of organic aerosols relative to black carbon during transport increasing absorption with age (Das et al., 2024). Our observations effectively capture plumes of similar origin at a further stage of ageing and vertical decoupling, approximately 5000 km downstream of the ORACLES measurement region. Layer altitudes (3-9 km) are also consistent with elevated smoke layers (3-8 km) documented during SAFARI-2000 (Abel et al., 2003; Haywood et al., 2003) and the "river of smoke" corridors characterized over the western SWIO (Flamant et al., 2022; Ranaivombola et al., 2025). The contribution of South American emissions to the lower tropospheric layer on September 25th is consistent with intercontinental transport routes documented by (Edwards et al., 2006) and (Duflot et al., 2010). The main advance of this study lies in providing, for the first time, vertically resolved optical characterization of BB plumes reaching Reunion Island through combined multiwavelength Raman lidar, sun-photometry, and transport modelling, extending the geographical reach of these major campaigns into the eastern SWIO. Our results demonstrate that aerosol layers arriving in the SWIO can retain distinct vertical structures and source signatures after transport over several thousand kilometers.

Several limitations should be acknowledged. First, the Ångström exponent differences between layers provides only a qualitative indication of relative aerosol ageing, as Å is influenced by particle size, mixing state, and hygroscopic growth in addition to transport history (Fiebig et al., 2003; Hänel, 1976; Reid et al., 1998; Zieger et al., 2013). In the present study, relative humidity within the aerosol layers remained sufficiently low for hygroscopic swelling to be considered a negligible contributor, and the moderate Å values (1.32-1.60) suggest the plumes had not yet entered the extreme aging regime where backscatter- and extinction-related Å diverge significantly (Haarig et al., 2018; Ohneiser et al., 2020). Second, the spatial averaging box used for CAMS validation incorporates surrounding ocean, which can inflate sea-salt contributions and introduce model–observation discrepancies. Regarding FLEXPART validation by FTIR, the limited vertical resolution of FTIR retrievals means this comparison primarily validates the overall vertical distribution of transported CO rather than the detailed structure of individual aerosol layers. Finally, this study focuses on a single month and two representative case studies; longer observational records will be required to quantify the climatological frequency and variability of the transport regimes identified.

Despite these limitations, our results highlight the importance of the SWIO as a receptor region for major long-range smoke export corridors from multiple continents. They also demonstrate the value of Reunion Island as a strategic observatory capable of documenting the full vertical structure and evolution of transported BB smoke plumes in the under sampled region of the SWIO. From a radiative forcing perspective, because absorbing BB aerosol layers were observed between 3 and 9 km altitude, such transport events are likely to influence regional radiative forcing, atmospheric stability, and potentially cloud development over the SWIO. Continued vertically resolved observations, combined with modelling, will be essential for constraining

https://doi.org/10.5194/egusphere-2026-3070
Preprint. Discussion started: 3 July 2026

aerosol-radiation interactions and improving the representation of long-range BB aerosol transport in regional and global climate models, especially in light of recent evidence for increasing fire activity in South America (Groenen et al., 2026).

Appendix A

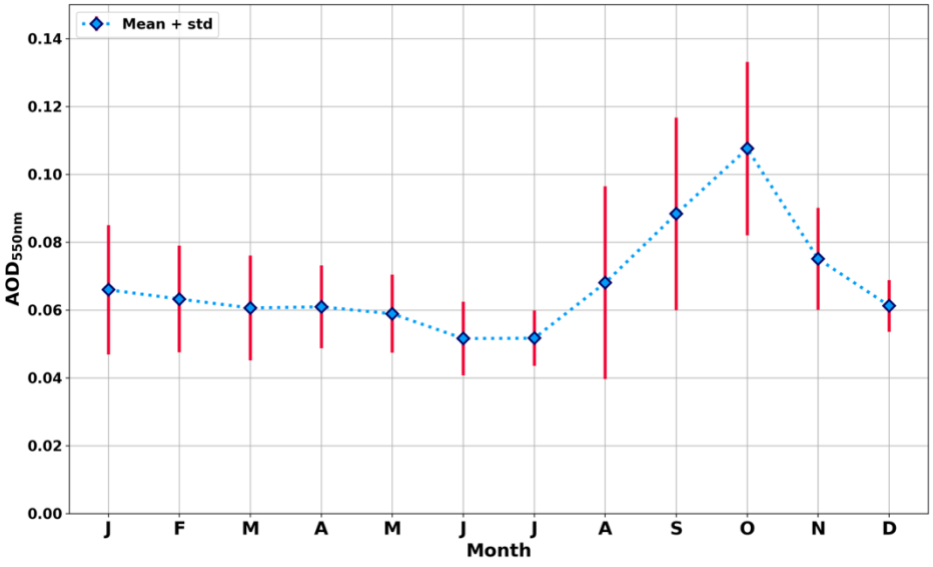

Figure A1: Mean (blue diamonds) and standard deviation (red lines) of AOD_{550} monthly climatology CIMEL sun-photometer measurements (AERONET network) above Saint-Denis between December 2003 and December 2024.

Video supplement.

An animated sequence of FLEXPART forward dispersion of CO emitted from South America and Southern Africa between September 16th and 26th, 2017 in terms of partial columns between 0 and 15 km, and vertical profiles at the latitude of 21.1° Maïdo observatory is available at https://doi.org/10.5446/73218 (Gantois, 2026).

Author contributions.

DG conducted this study with the help of AB, MS, VD and NB. DG and AB performed the aerosol related processing of the lidar measurements. GP performed the water vapor related processing of the lidar measurements. SE and NE performed the FLEXPART model analysis and provided the corresponding outputs. NB contributed to the discussions concerning the dynamical part of this paper and involving FLEXPART simulations. JMM, MM and CV provided us with the FTIR observations and with their expertise in this instrument. VD and NM were responsible for the LiO3T instrument and dataset, and VD and GP were responsible for the Li1200 instrument and dataset. NG provided MODIS and ERA5 figures. PC provided

CALIOP figures. PC and CF initiated the study and helped to implement the initial approach. All co-authors contributed to reviewing drafts of this manuscript.

Competing interests.

The authors declare that they have no conflict of interest.

Acknowledgments.

FLEXPART model simulations are cross-atmospheric research infrastructure services provided by ATMO-ACCESS (EU grant agreement No 101008004). SE and NE were funded by the same project. The computations/simulations were performed on resources provided by Sigma2 - the National Infrastructure for High Performance Computing and Data Storage in Norway. Eric Golubic, Patrick Hernandez, and Yann Hello are greatly thanked for the routine lidar measurements obtained at OPAR.

Financial support.

This research was funded by the European Union under Horizon Europe Grant Agreement 101086690. OPAR is presently funded by CNRS (INSU), Météo France, and Université de La Réunion, and managed by OSU-R (Observatoire des Sciences de l'Univers de La Réunion, UAR 3365). OPAR is supported by the French research infrastructure ACTRIS-FR (Aerosols, Clouds, and Trace gases Research InfraStructure - France) and by the French Center for Spatial Studies (CNES). This work was supported by the COST Action EARLICOST (CA24135), supported by COST (European Cooperation in Science and Technology). The authors acknowledge the support of the ANR through the OBS4CLIM project (ANR-21-ESRE-0013), and CNES through the projects EarthCARE-FR and EXTRA_SAT.

References.

Abel, S. J., Haywood, J. M., Highwood, E. J., Li, J., and Buseck, P. R.: Evolution of biomass burning aerosol properties from an agricultural fire in southern Africa, Geophysical Research Letters, 30, 2003GL017342, https://doi.org/10.1029/2003GL017342, 2003.

Ansmann, A., Wandinger, U., Riebesell, M., Weitkamp, C., and Michaelis, W.: Independent measurement of extinction and backscatter profiles in cirrus clouds by using a combined Raman elastic-backscatter lidar, Appl. Opt., 31, 7113, https://doi.org/10.1364/AO.31.007113, 1992.

Baray, J.-L., Courcoux, Y., Keckhut, P., Portafaix, T., Tulet, P., Cammas, J.-P., Hauchecorne, A., Godin-Beekmann, S., De Mazière, M., Hermans, C., Desmet, F., Sellegri, K., Colomb, A., Ramonet, M., Sciare, J., Vuillemin, C., Hoareau, C., Dionisi, D., Duflot, V., Vérèmes, H., Porteneuve, J., Gabarrot, F., Gaudo, T., Metzger, J.-M., Payen, G., Leclair De Bellevue, J., Barthe,

https://doi.org/10.5194/egusphere-2026-3070
Preprint. Discussion started: 3 July 2026

C., Posny, F., Abchiche, A., Delmas, R., and Ricaud, P.: Maïdo observatory: a new high-altitude station facility at Reunion Island (21° S, 55° E) for long-term atmospheric remote sensing and in situ measurements, Atmospheric Measurement Techniques, 6, 2865–2877, https://doi.org/10.5194/amt-6-2865-2013, 2013.

Benedetti, A., Morcrette, J.-J., Boucher, O., Dethof, A., Engelen, R. J., Fisher, M., Flentje, H., Huneeus, N., Jones, L., Kaiser, J. W., Kinne, S., Mangold, A., Razinger, M., Simmons, A. J., and Suttie, M.: Aerosol analysis and forecast in the European Centre for Medium-Range Weather Forecasts Integrated Forecast System: 2. Data assimilation, Journal of Geophysical Research: Atmospheres, 114, https://doi.org/10.1029/2008JD011115, 2009.

Chazette, P.: Raman lidar-derived aerosol optical properties and classification during the FENNEC experiment – Coherence with CAMS data, https://doi.org/10.5194/egusphere-2026-765, 11 March 2026.

Chazette, P., Flamant, C., Totems, J., Gaetani, M., Smith, G., Baron, A., Landsheere, X., Desboeufs, K., Doussin, J.-F., and Formenti, P.: Evidence of the complexity of aerosol transport in the lower troposphere on the Namibian coast during AEROCLO-sA, Atmos. Chem. Phys., 19, 14979–15005, https://doi.org/10.5194/acp-19-14979-2019, 2019.

Chu, D. A., Kaufman, Y. J., Ichoku, C., Remer, L. A., Tanré, D., and Holben, B. N.: Validation of MODIS aerosol optical depth retrieval over land, Geophysical Research Letters, 29, https://doi.org/10.1029/2001GL013205, 2002.

Das, S., Colarco, P. R., Bian, H., and Gassó, S.: Improved simulations of biomass burning aerosol optical properties and lifetimes in the NASA GEOS Model during the ORACLES-I campaign, Atmos. Chem. Phys., 24, 4421–4449, https://doi.org/10.5194/acp-24-4421-2024, 2024.

Duflot, V., Dils, B., Baray, J. L., De Mazière, M., Attié, J. L., Vanhaelewyn, G., Senten, C., Vigouroux, C., Clain, G., and Delmas, R.: Analysis of the origin of the distribution of CO in the subtropical southern Indian Ocean in 2007, J. Geophys. Res., 115, D22106, https://doi.org/10.1029/2010JD013994, 2010.

Duflot, V., Bègue, N., Pouliquen, M.-L., Goloub, P., and Metzger, J.-M.: Aerosols on the Tropical Island of La Réunion (21°S, 55°E): Assessment of Climatology, Origin of Variability and Trend, Remote Sensing, 14, 4945, https://doi.org/10.3390/rs14194945, 2022.

Edwards, D. P., Emmons, L. K., Gille, J. C., Chu, A., Attié, J.-L., Giglio, L., Wood, S. W., Haywood, J., Deeter, M. N., Massie, S. T., Ziskin, D. C., and Drummond, J. R.: Satellite-observed pollution from Southern Hemisphere biomass burning, J. Geophys. Res., 111, D14312, https://doi.org/10.1029/2005JD006655, 2006.

Fiebig, M., Stohl, A., Wendisch, M., Eckhardt, S., and Petzold, A.: Dependence of solar radiative forcing of forest fire aerosol on ageing and state of mixture, Atmos. Chem. Phys., 3, 881–891, https://doi.org/10.5194/acp-3-881-2003, 2003.

Flamant, C., Gaetani, M., Chaboureau, J.-P., Chazette, P., Cuesta, J., Piketh, S. J., and Formenti, P.: Smoke in the river: an Aerosols, Radiation and Clouds in southern Africa (AEROCLO-sA) case study, Atmos. Chem. Phys., 22, 5701–5724, https://doi.org/10.5194/acp-22-5701-2022, 2022.

Floutsi, A. A., Baars, H., Engelmann, R., Althausen, D., Ansmann, A., Bohlmann, S., Heese, B., Hofer, J., Kanitz, T., Haarig, M., Ohneiser, K., Radenz, M., Seifert, P., Skupin, A., Yin, Z., Abdullaev, S. F., Komppula, M., Filioglou, M., Giannakaki, E., Stachlewska, I. S., Janicka, L., Bortoli, D., Marinou, E., Amiridis, V., Gialitaki, A., Mamouri, R.-E., Barja, B., and Wandinger,

U.: DeLiAn – a growing collection of depolarization ratio, lidar ratio and Ångström exponent for different aerosol types and mixtures from ground-based lidar observations, Atmos. Meas. Tech., 16, 2353–2379, https://doi.org/10.5194/amt-16-2353-2023, 2023.

Formenti, P., D'Anna, B., Flamant, C., Mallet, M., Piketh, S. J., Schepanski, K., Waquet, F., Auriol, F., Brogniez, G., Burnet, F., Chaboureau, J.-P., Chauvigné, A., Chazette, P., Denjean, C., Desboeufs, K., Doussin, J.-F., Elguindi, N., Feuerstein, S., Gaetani, M., Giorio, C., Klopper, D., Mallet, M. D., Nabat, P., Monod, A., Solmon, F., Namwoonde, A., Chikwililwa, C., Mushi, R., Welton, E. J., and Holben, B.: The Aerosols, Radiation and Clouds in Southern Africa Field Campaign in Namibia: Overview, Illustrative Observations, and Way Forward, Bulletin of the American Meteorological Society, 100, 1277–1298, https://doi.org/10.1175/BAMS-D-17-0278.1, 2019.

Forster, C., Stohl, A., and Seibert, P.: Parameterization of Convective Transport in a Lagrangian Particle Dispersion Model and Its Evaluation, Journal of Applied Meteorology and Climatology, 46, 403–422, https://doi.org/10.1175/JAM2470.1, 2007.

Gantois, D.: Entwined long-range transports of biomass burning aerosols over the South-West Indian Ocean: a case study of aerosol river in September 2017, https://doi.org/10.5446/73218, 2026.

Gantois, D., Payen, G., Sicard, M., Duflot, V., Bègue, N., Marquestaut, N., Portafaix, T., Godin Beekmann, S., Hernandez, P., and Golubic, E.: Multiwavelength aerosol lidars at Maïdo Observatory, https://doi.org/https://doi.org/10.26171/rwcm-q370, 2024.

Garstang, M., Tyson, P. D., Swap, R., Edwards, M., Kållberg, P., and Lindesay, J. A.: Horizontal and vertical transport of air over southern Africa, J. Geophys. Res., 101, 23721–23736, https://doi.org/10.1029/95JD00844, 1996.

Giles, D. M., Sinyuk, A., Sorokin, M. G., Schafer, J. S., Smirnov, A., Slutsker, I., Eck, T. F., Holben, B. N., Lewis, J. R., Campbell, J. R., Welton, E. J., Korkin, S. V., and Lyapustin, A. I.: Advancements in the Aerosol Robotic Network (AERONET) Version 3 database – automated near-real-time quality control algorithm with improved cloud screening for Sun photometer aerosol optical depth (AOD) measurements, Atmospheric Measurement Techniques, 12, 169–209, https://doi.org/10.5194/amt-12-169-2019, 2019.

Groenen, N., Sicard, M., and Nabat, P.: Characteristics and trend of the wildfire activity in the Southern Hemisphere (2004-2024), Science of The Total Environment, 2026.

Haarig, M., Ansmann, A., Baars, H., Jimenez, C., Veselovskii, I., Engelmann, R., and Althausen, D.: Depolarization and lidar ratios at 355, 532, and 1064 nm and microphysical properties of aged tropospheric and stratospheric Canadian wildfire smoke, Atmos. Chem. Phys., 18, 11847–11861, https://doi.org/10.5194/acp-18-11847-2018, 2018.

Hänel, G.: The Properties of Atmospheric Aerosol Particles as Functions of the Relative Humidity at Thermodynamic Equilibrium with the Surrounding Moist Air, in: Advances in Geophysics, vol. 19, Elsevier, 73–188, https://doi.org/10.1016/S0065-2687(08)60142-9, 1976.

Hannigan, J., Palm, M., Jones, N., Ortega, I., Langerock, B., Mahieu, E., Zhou, M., and Smale, D.: SFIT4 Line-by-line nonlinear spectral fitting software: version 0.9.4, , 442838 kb, https://doi.org/10.18758/EIJXNQWO, 2024.

https://doi.org/10.5194/egusphere-2026-3070
Preprint. Discussion started: 3 July 2026

Haywood, J. M., Osborne, S. R., Francis, P. N., Keil, A., Formenti, P., Andreae, M. O., and Kaye, P. H.: The mean physical and optical properties of regional haze dominated by biomass burning aerosol measured from the C-130 aircraft during SAFARI 2000, J. Geophys. Res., 108, 2002JD002226, https://doi.org/10.1029/2002JD002226, 2003.

Hersbach, H., Bell, B., Berrisford, P., Hirahara, S., Horányi, A., Muñoz-Sabater, J., Nicolas, J., Peubey, C., Radu, R., Schepers, D., Simmons, A., Soci, C., Abdalla, S., Abellan, X., Balsamo, G., Bechtold, P., Biavati, G., Bidlot, J., Bonavita, M., De Chiara, G., Dahlgren, P., Dee, D., Diamantakis, M., Dragani, R., Flemming, J., Forbes, R., Fuentes, M., Geer, A., Haimberger, L., Healy, S., Hogan, R. J., Hólm, E., Janisková, M., Keeley, S., Laloyaux, P., Lopez, P., Lupu, C., Radnoti, G., De Rosnay, P., Rozum, I., Vamborg, F., Villaume, S., and Thépaut, J.: The ERA5 global reanalysis, Quart J Royal Meteoro Soc, 146, 1999–2049, https://doi.org/10.1002/qj.3803, 2020.

Holben, B. N., Eck, T. F., Slutsker, I., Tanré, D., Buis, J. P., Setzer, A., Vermote, E., Reagan, J. A., Kaufman, Y. J., Nakajima, T., Lavenu, F., Jankowiak, I., and Smirnov, A.: AERONET—A Federated Instrument Network and Data Archive for Aerosol Characterization, Remote Sensing of Environment, 66, 1–16, https://doi.org/10.1016/S0034-4257(98)00031-5, 1998.

Inness, A., Ades, M., Agustí-Panareda, A., Barré, J., Benedictow, A., Blechschmidt, A.-M., Dominguez, J. J., Engelen, R., Eskes, H., Flemming, J., Huijnen, V., Jones, L., Kipling, Z., Massart, S., Parrington, M., Peuch, V.-H., Razinger, M., Remy, S., Schulz, M., and Suttie, M.: The CAMS reanalysis of atmospheric composition, Atmos. Chem. Phys., 19, 3515–3556, https://doi.org/10.5194/acp-19-3515-2019, 2019.

Kaiser, J. W., Heil, A., Andreae, M. O., Benedetti, A., Chubarova, N., Jones, L., Morcrette, J.-J., Razinger, M., Schultz, M. G., Suttie, M., and Van Der Werf, G. R.: Biomass burning emissions estimated with a global fire assimilation system based on observed fire radiative power, Biogeosciences, 9, 527–554, https://doi.org/10.5194/bg-9-527-2012, 2012.

Kim, M.-H., Omar, A. H., Tackett, J. L., Vaughan, M. A., Winker, D. M., Trepte, C. R., Hu, Y., Liu, Z., Poole, L. R., Pitts, M. C., Kar, J., and Magill, B. E.: The CALIPSO version 4 automated aerosol classification and lidar ratio selection algorithm, Atmos. Meas. Tech., 11, 6107–6135, https://doi.org/10.5194/amt-11-6107-2018, 2018.

King, M. D., Kaufman, Y. J., Menzel, W. P., and Tanre, D.: Remote sensing of cloud, aerosol, and water vapor properties from the moderate resolution imaging spectrometer (MODIS), IEEE Trans. Geosci. Remote Sensing, 30, 2–27, https://doi.org/10.1109/36.124212, 1992.

Klett, J. D.: Lidar inversion with variable backscatter/extinction ratios, Appl. Opt., 24, 1638, https://doi.org/10.1364/AO.24.001638, 1985.

Lu, Z., Liu, X., Zhang, Z., Zhao, C., Meyer, K., Rajapakshe, C., Wu, C., Yang, Z., and Penner, J. E.: Biomass smoke from southern Africa can significantly enhance the brightness of stratocumulus over the southeastern Atlantic Ocean, Proc. Natl. Acad. Sci. U.S.A., 115, 2924–2929, https://doi.org/10.1073/pnas.1713703115, 2018.

Mangold, A., De Backer, H., De Paepe, B., Dewitte, S., Chiapello, I., Derimian, Y., Kacenelenbogen, M., Léon, J.-F., Huneeus, N., Schulz, M., Ceburnis, D., O'Dowd, C., Flentje, H., Kinne, S., Benedetti, A., Morcrette, J.-J., and Boucher, O.: Aerosol analysis and forecast in the European Centre for Medium-Range Weather Forecasts Integrated Forecast System: 3. Evaluation by means of case studies, Journal of Geophysical Research: Atmospheres, 116, https://doi.org/10.1029/2010JD014864, 2011.

https://doi.org/10.5194/egusphere-2026-3070
Preprint. Discussion started: 3 July 2026

Mascaut, F., Pujol, O., Verreyken, B., Peroni, R., Metzger, J. M., Blarel, L., Podvin, T., Goloub, P., Sellegri, K., Thornberry, T., Duflot, V., Tulet, P., and Brioude, J.: Aerosol characterization in an oceanic context around Reunion Island (AEROMARINE field campaign), Atmospheric Environment, 268, 118770, https://doi.org/10.1016/j.atmosenv.2021.118770, 2022.

Morcrette, J.-J., Boucher, O., Jones, L., Salmond, D., Bechtold, P., Beljaars, A., Benedetti, A., Bonet, A., Kaiser, J. W., Razinger, M., Schulz, M., Serrar, S., Simmons, A. J., Sofiev, M., Suttie, M., Tompkins, A. M., and Untch, A.: Aerosol analysis and forecast in the European Centre for Medium-Range Weather Forecasts Integrated Forecast System: Forward modeling, Journal of Geophysical Research: Atmospheres, 114, https://doi.org/10.1029/2008JD011235, 2009.

Ohneiser, K., Ansmann, A., Baars, H., Seifert, P., Barja, B., Jimenez, C., Radenz, M., Teisseire, A., Floutsi, A., Haarig, M., Foth, A., Chudnovsky, A., Engelmann, R., Zamorano, F., Bühl, J., and Wandinger, U.: Smoke of extreme Australian bushfires observed in the stratosphere over Punta Arenas, Chile, in January 2020: optical thickness, lidar ratios, and depolarization ratios at 355 and 532 nm, Atmos. Chem. Phys., 20, 8003–8015, https://doi.org/10.5194/acp-20-8003-2020, 2020.

Pisso, I., Sollum, E., Grythe, H., Kristiansen, N. I., Cassiani, M., Eckhardt, S., Arnold, D., Morton, D., Thompson, R. L., Groot Zwaaftink, C. D., Evangeliou, N., Sodemann, H., Haimberger, L., Henne, S., Brunner, D., Burkhart, J. F., Fouilloux, A., Brioude, J., Philipp, A., Seibert, P., and Stohl, A.: The Lagrangian particle dispersion model FLEXPART version 10.4, Geosci. Model Dev., 12, 4955–4997, https://doi.org/10.5194/gmd-12-4955-2019, 2019.

Ramanathan, V., Crutzen, P. J., Lelieveld, J., Mitra, A. P., Althausen, D., Anderson, J., Andreae, M. O., Cantrell, W., Cass, G. R., Chung, C. E., Clarke, A. D., Coakley, J. A., Collins, W. D., Conant, W. C., Dulac, F., Heintzenberg, J., Heymsfield, A. J., Holben, B., Howell, S., Hudson, J., Jayaraman, A., Kiehl, J. T., Krishnamurti, T. N., Lubin, D., McFarquhar, G., Novakov, T., Ogren, J. A., Podgorny, I. A., Prather, K., Priestley, K., Prospero, J. M., Quinn, P. K., Rajeev, K., Rasch, P., Rupert, S., Sadourny, R., Satheesh, S. K., Shaw, G. E., Sheridan, P., and Valero, F. P. J.: Indian Ocean Experiment: An integrated analysis of the climate forcing and effects of the great Indo-Asian haze, J. Geophys. Res., 106, 28371–28398, https://doi.org/10.1029/2001JD900133, 2001.

Ranaivombola, M., Bègue, N., Bencherif, H., Millet, T., Sivakumar, V., Duflot, V., Baron, A., Mbatha, N., Piketh, S., Formenti, P., and Goloub, P.: Aerosol Optical Properties and Types over Southern Africa and Reunion Island Determined from Ground-Based and Satellite Observations over a 13-Year Period (2008–2021), Remote Sensing, 15, 1581, https://doi.org/10.3390/rs15061581, 2023.

Ranaivombola, M., Bègue, N., Vaz Peres, L., Fazel-Rastgar, F., Sivakumar, V., Krysztofiak, G., Berthet, G., Jegou, F., Piketh, S., and Bencherif, H.: Characterization of aerosol optical depth (AOD) anomalies in September and October 2022 over Skukuza in South Africa, Atmos. Chem. Phys., 25, 3519–3540, https://doi.org/10.5194/acp-25-3519-2025, 2025.

Redemann, J., Wood, R., Zuidema, P., Doherty, S. J., Luna, B., LeBlanc, S. E., Diamond, M. S., Shinozuka, Y., Chang, I. Y., Ueyama, R., Pfister, L., Ryoo, J.-M., Dobracki, A. N., Da Silva, A. M., Longo, K. M., Kacenelenbogen, M. S., Flynn, C. J., Pistone, K., Knox, N. M., Piketh, S. J., Haywood, J. M., Formenti, P., Mallet, M., Stier, P., Ackerman, A. S., Bauer, S. E., Fridlind, A. M., Carmichael, G. R., Saide, P. E., Ferrada, G. A., Howell, S. G., Freitag, S., Cairns, B., Holben, B. N.,

https://doi.org/10.5194/egusphere-2026-3070
Preprint. Discussion started: 3 July 2026

Knobelspiesse, K. D., Tanelli, S., L'Ecuyer, T. S., Dzambo, A. M., Sy, O. O., McFarquhar, G. M., Poellot, M. R., Gupta, S., O'Brien, J. R., Nenes, A., Kacarab, M., Wong, J. P. S., Small-Griswold, J. D., Thornhill, K. L., Noone, D., Podolske, J. R., Schmidt, K. S., Pilewskie, P., Chen, H., Cochrane, S. P., Sedlacek, A. J., Lang, T. J., Stith, E., Segal-Rozenhaimer, M., Ferrare, R. A., Burton, S. P., Hostetler, C. A., Diner, D. J., Seidel, F. C., Platnick, S. E., Myers, J. S., Meyer, K. G., Spangenberg, D. A., Maring, H., and Gao, L.: An overview of the ORACLES (ObseRvations of Aerosols above CLouds and their intEractionS) project: aerosol–cloud–radiation interactions in the southeast Atlantic basin, Atmos. Chem. Phys., 21, 1507–1563, https://doi.org/10.5194/acp-21-1507-2021, 2021.

Reid, J. S., Hobbs, P. V., Ferek, R. J., Blake, D. R., Martins, J. V., Dunlap, M. R., and Liousse, C.: Physical, chemical, and optical properties of regional hazes dominated by smoke in Brazil, J. Geophys. Res., 103, 32059–32080, https://doi.org/10.1029/98JD00458, 1998.

Rodgers, C. D.: Inverse Methods for Atmospheric Sounding: Theory and Practice, WORLD SCIENTIFIC, https://doi.org/10.1142/3171, 2000.

Rodgers, C. D. and Connor, B. J.: Intercomparison of remote sounding instruments, J. Geophys. Res., 108, 2002JD002299, https://doi.org/10.1029/2002JD002299, 2003.

Salomonson, V. V., Barnes, W. L., Maymon, P. W., Montgomery, H. E., and Ostrow, H.: MODIS: advanced facility instrument for studies of the Earth as a system, IEEE Trans. Geosci. Remote Sensing, 27, 145–153, https://doi.org/10.1109/36.20292, 1989.

Schmid, B., Redemann, J., Russell, P. B., Hobbs, P. V., Hlavka, D. L., McGill, M. J., Holben, B. N., Welton, E. J., Campbell, J. R., Torres, O., Kahn, R. A., Diner, D. J., Helmlinger, M. C., Chu, D. A., Robles-Gonzalez, C., and De Leeuw, G.: Coordinated airborne, spaceborne, and ground-based measurements of massive thick aerosol layers during the dry season in southern Africa, J. Geophys. Res., 108, 2002JD002297, https://doi.org/10.1029/2002JD002297, 2003.

Senten, C., De Mazière, M., Dils, B., Hermans, C., Kruglanski, M., Neefs, E., Scolas, F., Vandaele, A. C., Vanhaelewyn, G., Vigouroux, C., Carleer, M., Coheur, P. F., Fally, S., Barret, B., Baray, J. L., Delmas, R., Leveau, J., Metzger, J. M., Mahieu, E., Boone, C., Walker, K. A., Bernath, P. F., and Strong, K.: Technical Note: New ground-based FTIR measurements at Ile de La Réunion: observations, error analysis, and comparisons with independent data, Atmos. Chem. Phys., 8, 3483–3508, https://doi.org/10.5194/acp-8-3483-2008, 2008.

Simoneit, B. R. T.: Biomass burning — a review of organic tracers for smoke from incomplete combustion, Applied Geochemistry, 17, 129–162, https://doi.org/10.1016/S0883-2927(01)00061-0, 2002.

Smirnov, A., Holben, B. N., Eck, T. F., Dubovik, O., and Slutsker, I.: Cloud-Screening and Quality Control Algorithms for the AERONET Database, Remote Sensing of Environment, 73, 337–349, https://doi.org/10.1016/S0034-4257(00)00109-7, 2000.

Stohl, A., Forster, C., Frank, A., Seibert, P., and Wotawa, G.: Technical note: The Lagrangian particle dispersion model FLEXPART version 6.2, Atmos. Chem. Phys., 5, 2461–2474, https://doi.org/10.5194/acp-5-2461-2005, 2005.

https://doi.org/10.5194/egusphere-2026-3070
Preprint. Discussion started: 3 July 2026

765 Swap, R. J., Annegarn, H. J., Suttles, J. T., King, M. D., Platnick, S., Privette, J. L., and Scholes, R. J.: Africa burning: A
766 thematic analysis of the Southern African Regional Science Initiative (SAFARI 2000): AFRICA BURNING, SAFARI 2000,
767 J. Geophys. Res., 108, n/a-n/a, https://doi.org/10.1029/2003JD003747, 2003.
768 Tackett, J. L., Kar, J., Vaughan, M. A., Getzewich, B. J., Kim, M.-H., Vernier, J.-P., Omar, A. H., Magill, B. E., Pitts, M. C.,
769 and Winker, D. M.: The CALIPSO version 4.5 stratospheric aerosol subtyping algorithm, Atmos. Meas. Tech., 16, 745–768,
770 https://doi.org/10.5194/amt-16-745-2023, 2023.
771 Thompson, A. M., Pickering, K. E., McNamara, D. P., Schoeberl, M. R., Hudson, R. D., Kim, J. H., Browell, E. V., Kirchhoff,
772 V. W. J. H., and Nganga, D.: Where did tropospheric ozone over southern Africa and the tropical Atlantic come from in
773 October 1992? Insights from TOMS, GTE TRACE A, and SAFARI 1992, J. Geophys. Res., 101, 24251–24278,
774 https://doi.org/10.1029/96JD01463, 1996.
775 Van Der Werf, G. R., Randerson, J. T., Giglio, L., Van Leeuwen, T. T., Chen, Y., Rogers, B. M., Mu, M., Van Marle, M. J.
776 E., Morton, D. C., Collatz, G. J., Yokelson, R. J., and Kasibhatla, P. S.: Global fire emissions estimates during 1997–2016,
777 Earth Syst. Sci. Data, 9, 697–720, https://doi.org/10.5194/essd-9-697-2017, 2017.
778 Vérèmes, H., Payen, G., Keckhut, P., Duflot, V., Baray, J.-L., Cammas, J.-P., Evan, S., Posny, F., Körner, S., and Bosser, P.:
779 Validation of the Water Vapor Profiles of the Raman Lidar at the Maïdo Observatory (Reunion Island) Calibrated with Global
780 Navigation Satellite System Integrated Water Vapor, Atmosphere, 10, 713, https://doi.org/10.3390/atmos10110713, 2019.
781 Wandinger, U., Müller, D., Böckmann, C., Althausen, D., Matthias, V., Bösenberg, J., Weiß, V., Fiebig, M., Wendisch, M.,
782 Stohl, A., and Ansmann, A.: Optical and microphysical characterization of biomass- burning and industrial-pollution aerosols
783 from- multiwavelength lidar and aircraft measurements, J. Geophys. Res., 107, https://doi.org/10.1029/2000JD000202, 2002.
784 Winker, D. M., Hunt, W. H., and McGill, M. J.: Initial performance assessment of CALIOP, Geophysical Research Letters,
785 34, 2007GL030135, https://doi.org/10.1029/2007GL030135, 2007.
786 Young, S. A. and Vaughan, M. A.: The Retrieval of Profiles of Particulate Extinction from Cloud-Aerosol Lidar Infrared
787 Pathfinder Satellite Observations (CALIPSO) Data: Algorithm Description, Journal of Atmospheric and Oceanic Technology,
788 26, 1105–1119, https://doi.org/10.1175/2008JTECHA1221.1, 2009.
789 Zhou, M., Langerock, B., Vigouroux, C., Wang, P., Hermans, C., Stiller, G., Walker, K. A., Dutton, G., Mahieu, E., and De
790 Mazière, M.: Ground-based FTIR retrievals of SF_6 on Reunion Island, Atmos. Meas. Tech., 11, 651–662,
791 https://doi.org/10.5194/amt-11-651-2018, 2018.
792 Zieger, P., Fierz-Schmidhauser, R., Weingartner, E., and Baltensperger, U.: Effects of relative humidity on aerosol light
793 scattering: results from different European sites, Atmos. Chem. Phys., 13, 10609–10631, https://doi.org/10.5194/acp-13-
794 10609-2013, 2013.
795